Molecular Self-Assembly at Bare Semiconductor Surfaces: Cooperative Substrate−Molecule Effects in Octadecanethiolate Monolayer Assemblies on GaAs(111), (110), and (100)

Christine L. McGuiness,[†,¶] Gregory A. Diehl,[†] Daniel Blasini,[‡] Detlef-M. Smilgies,[§] M. Zhu,[∥] Nitin Samarth,[∥] Tobias Weidner,[⊥,#] Nirmalya Ballav,[⊥] Michael Zharnikov,[⊥,*] and David L. Allara[†,*]

[†]Departments of Chemistry and Materials Science & Engineering, The Pennsylvania State University, 104 Chemistry Building, University Park, Pennsylvania 16801, [‡]Department of Chemistry, Cornell University, Baker Laboratory, Ithaca, New York 14853, [§]Cornell High Energy Synchrotron Source, 200 L Wilson Lab, Ithaca, New York 14853, [⊥]Angewandte Physikalische Chemie, Universität Heidelberg, Im Neuenheimer Feld 253, D-69120 Heildelberg, Germany, and [∥]Department of Physics, The Pennsylvania State University, 104 Davey, University Park, Pennsylvania 16801. [¶]Present address: Plextronics, Inc., 2180 William Pitt Way, Pittsburgh, Pennsylvania 15238. [#]Present address: National ESCA and Surface Analysis Center for Biomedical Problems (NESAC/BIO), University of Washington, Seattle, Washington 98195.

ABSTRACT The structures of self-assembled monolayers formed by chemisorption of octadecanethiol onto the surfaces of GaAs(001), (110), (111-A)-Ga, and (111-B)-As have been characterized in detail by a combination of X-ray photoelectron, near-edge X-ray absorption fine structure, and infrared spectroscopies and grazing incidence X-ray diffraction. In all cases, the molecular lattices are ordered with hexagonal symmetry, even for the square and rectangular intrinsic substrate (001) and (110) lattices, and the adsorbate lattice spacings are all incommensurate with their respective intrinsic substrate lattices. These results definitively show that the monolayer organization is driven by intermolecular packing forces to assemble in a hexagonal motif, such as would occur in the approach to a limit for an energetically featureless surface. The accompanying introduction of strain into the soft substrate surface lattice *via* strong S substrate bonds forces the soft substrate lattice to compliantly respond, introducing quasi-2D strain. A notably poorer organization for the (111-A)-Ga case compared to the (111-B)-As and other faces indicates that that the Ga-terminated surface lattice is more resistant to adsorbate packing-induced stress. Overall, the results show that surface molecular self-assembly must be considered as a strongly cooperative process between the substrate surface and the adsorbate and that inorganic substrate surfaces should not be considered as necessarily rigid when strong intermolecular adsorbate packing forces are operative.

KEYWORDS: GaAs · self-assembly · self-assembled monolayers · grazing incidence X-ray diffraction · chemisorption · semiconductor surfaces

Unraveling the structural details of assemblies of organic molecules adsorbed on surfaces is an essential element in understanding a wide range of important surface and interface phenomena, both in naturally occurring and synthetic systems, and is critical for accelerating the design and development of new types of functional surfaces and interfaces. Examples range widely across wetting behavior,[1−4] molecular electronic devices,[5,6] protein and cellular adsorption,[7,8] and phase behavior of model biomembrane systems.[9,10]

A key issue in surface self-assembly (SSA) revolves around the correlation between the chemical and structural elements of the initial adsorbent surface and isolated molecules and the final state which arises after adsorption under some specified condition. One can view SSA loosely as a quasi-2D subset of the general hierarchical self-assembly process[11] in which molecules self-organize across a plane containing a distribution of pinning sites, with the restriction that in many cases the adsorption process is highly irreversible, leading to a final structure dominated by kinetic paths with limited self-ordering. In more detail, the final structure develops in processes guided by a balance between intermolecular packing forces, substrate−molecule bonding energetics, and molecular ensemble−substrate lattice matching.[12,13]

In general, SSA final states fit within three limiting cases that depend on the molecular mobility on the surface, which in turn is controlled primarily by the depths of the energy wells for adsorbate−pinning site coupling. At one limit is the example of alkyl chains grafted at Si(111)-H surfaces *via* covalent Si−C bonds.[14,15] In this case, the molecules are strongly bonded to the silicon surface in deep wells with energies $\gg k_BT$, thus eliminating adsorbate translational mobility. The low mobility and large

*Address correspondence to dla3@psu.edu.

Received for review March 7, 2010 and accepted May 09, 2010.

Published online May 19, 2010. 10.1021/nn1004638

mismatch in molecular sizes and substrate lattice spacings result in incomplete coverage, commensurate superlattice molecular films with extremely short-range order in which inherent defects will not anneal out.

At the other limit, molecules are decoupled from the pinning lattice (template) and exhibit large surface mobility, exemplified by cases such as Langmuir-type surfactant assembly at the air/water interface, physisorbed sexiphenyl molecules on alkali halide surfaces,[16] or wax hydrocarbon monolayers absorbed on silicon wafers.[17] One example of this for solid surfaces is *n*-alkylsiloxane self-assembly on highly hydrated SiO_2 surfaces.[18−20] In this case, the assembly approaches a limit in which self-organization is driven by intermolecular packing forces, resulting in translational and orientation order with dense packing at a 20.3 Å^2/molecule reciprocal areal density.[21] An intermediate case between these limits is represented by alkanethiolates on Au(111) surfaces[22−24] in which the S−Au bonds pin the molecules into a commensurate overlayer superlattice.[25−28] Although the initial formation of these monolayers results in short translational order[29] due to surface mobility limitations,[30,31] long-range translational order can be achieved over time[32] or by thermal annealing.[33] Of the many organic monolayer systems reported, the structure and molecular organization of organo-thiolate self-assembled monolayers (SAM) adsorbed on Au surfaces have been the most widely studied, in part, because their intermediary characteristics of assembly enable facile formation of dense, highly conformal molecular films that can be applied and utilized in many applications.

The use of organothiolate SAMs on Au, or other metal, surfaces[12] is technologically limiting, and as a result, self-assembling chemistries on semiconducting surfaces have also been investigated, particularly on the group IV[15,34−37] and III−V semiconductors, important for electronic device applications.[38−51] The group IV substrates, as mentioned above, involve high-energy bonds which prevent long-range self-organization of the grafted molecules,[15,34−37] but in the case of alkanethiolates adsorbed on GaAs(001) surfaces, it is now recognized that translationally ordered SAMs can be formed, as demonstrated by our recent report of pseudohexagonal overlayers for $n > 15$ in $C_nH_{2n+1}S$-.[52] These results showed that the inherent mismatch between the substrate spacing and symmetry of the square lattice pinning sites and the ideal molecular lattice spacing and hexagonal symmetry for crystalline packing of vertically oriented chains was overcome by distortion of the (001) surface lattice to accommodate a preferred molecular packing incommensurate with the intrinsic square lattice. It was observed, however, that in spite of the surface lattice strain, there is a strong tendency for the SAM domains to align along the intrinsic substrate [1$\bar{1}$0] crystal directions, indicating that the underlying (001) substrate does impart some influence on the direction of the final molecular unit cell.

With these observations in mind, we wanted to understand how the substrate surface atom arrangements on different GaAs crystal faces might be manifested in structural differences of the corresponding SAMs and, in particular, look for the interplay between the potentially competing forces of molecular packing lattice strain. It already has been shown for the case of alkanethiols on Au how different crystal termination faces result in important differences in the structure of the SAMs. For example, high-coverage SAMs formed on {111} textured polycrystalline and single-crystal fcc(111) surfaces are found to adopt ∼26−30° chain tilts with a $n(\sqrt{3} \times \sqrt{3})R30°$ lattice structure (n = 1,2).[12,53−57] In comparison, SAMs formed on the fcc(100) square lattice surface adopt a ∼14° chain tilt and either an incommensurate or $c(2 \times 2)$ lattice spacings.[53,58] The ∼14° tilt is similar to alkanethiolate SAM conformation formed on Ag, Pt, Pd, and Cu polycrystalline {111} surfaces[12,59−61] as well as alkanethiolates formed on the GaAs(001) surfaces.[62] On the Au(110) surface, the alkanethiolate molecules adopt a ∼37° chain tilt with a commensurate $c(2 \times 2)$ structure.[63] Following this approach, we were interested in studying analogous trends of the alkanethiolate molecules adsorbed on the different low-index crystallographic faces of GaAs.

On the low-index crystallographic faces of GaAs, (001), (110), (111-A, Ga-terminated), and (111-B, As-terminated), structural differences in the monolayer organization are also expected not only because of differences in the lattice arrangements but also due to differences in the surface chemistries.[64] The unreconstructed (001) GaAs surface is a polar, square lattice, terminated by either Ga or As atoms, each with two back bonds and two unsaturated dangling bonds.[64] The drive to minimize the chemical instability imparted by the dangling bonds results in the prevalence of many (001) reconstructions, usually based on dimer row structures.[65] The (001) surface is different from the (110) rectangular lattice surface both structurally and chemically. The (110) surface is the most chemically stable of the low index surfaces due to its nonpolarity, which arises from equal Ga and As atoms present at the surface.[64] These characteristics also make it the dominant cleavage plane.[66,67]

The other low-index surface planes, (111-A)-Ga and (111-B)-As, are structurally different from either the (001) or (110) surfaces. Both the (111-A) and (111-B) surfaces have a hexagonal polar surface terminated in Ga or As, respectively. Unlike the polar (001) surface, however, each Ga or As atom has only one dangling bond. Due to the fact that the Ga (As) atoms contribute $3e^-$ ($5e^-$) of the 8 electrons in the GaAs tetrahedral sp^3 bonds, when cleavage occurs, the Ga surface rehybridizes to three filled sp^2 bonds, while the As atom will retain its sp^3 hybridization, with one lone pair.[64] As a result, the (111-A)-Ga surface is more stable than the

(111-B)-As surface and serves as the stop etch plane for the (111) orientation.[66,67]

Of the four low-index GaAs surfaces, alkanethiolate self- assembly has primarily been studied on the technologically relevant (001) surfaces.[38−50,68−72] In comparison, there are only a few known studies of the structure of organothiolate monolayers formed on the other low-index GaAs surfaces, and of these, only GaAs(110) has been investigated.[73−76] In one study using lateral force microscopy, octadecanethiolate (ODT) SAMs formed on (110) surfaces were found to form periodic rows 5.7 Å apart, rotated 55° to the other. A $c(2 \times 2)$ lattice structure with a chain tilt of 57.4° was proposed.[74] On an analogous III−V semiconductor surface, InP(110), the "upright" phase of dodecanethiolate monolayers formed by vapor dosing the surface was investigated by X-ray absorption near-edge fine structure spectroscopy (NEXAFS) and scanning tunneling microscopy (STM) and found to have a chain tilt of 34°, with the molecules tilted toward the [001] crystallographic direction.[77−79] No studies of the structures of organothiolate monolayers on any III−V semiconductor (111) surface are currently available. One recent study investigated organo-thiolate monolayer formation on Ge(111) surfaces and found that they form less robust SAMs compared to the same monolayers prepared on the Ge(100) surface.[36]

Since the specific atom structure and surface chemistry of each of the (001), (110), (111-A)-Ga, and (111-B)-As GaAs surfaces differ greatly from each other, our aim was to investigate the influence of substrate chemistry and lattice structure on SAM organization on GaAs surfaces. For an adsorbate, we chose octadecanethiol (ODT) molecules, known to form densely packed monolayers on GaAs(001) surfaces.[52] Using the same rigorous assembly conditions previously used for the (001) surface,[62] SAMs were formed on the (110), (111-A)-Ga, and (111-B)-As surfaces and then thoroughly characterized by a combination of liquid contact angle probe measurements, NEXAFS spectroscopy, infrared reflection spectroscopy (IRS), high-resolution X-ray photoelectron spectroscopy (HRXPS), and grazing incidence X-ray diffraction (GIXRD). The results show that the SAMs on (110) surfaces have similar structures to those reported for (001) surfaces, including highly hydrophobic and oleophobic wettabilities, a nearly identical near vertical molecular tilt and an incommensurate, pseudohexagonal unit cell, aligned along the intrinsic substrate [100] direction, in contrast to the $[1\bar{1}0]$ alignment for the SAM on the (001) surface. An important finding for the (111) surfaces is that hexagonal packed, highly organized SAMs form on the As-rich (111-B) surface, whereas low coverage poorly organized monolayers form on the Ga-terminated (111-A) surfaces, an indication that the Ga-terminated substrate surface is more resistant to accommodation to the preferred adsorbate ordering. Finally, SAM formation on *epi*-GaAs(001) surfaces with no step edges reveals no preferential alignment of the SAM domains with the intrinsic GaAs lattice, thus demonstrating that any correlations of the molecular domain alignment and intrinsic substrate lattice occur only through substrate step edges.

TABLE 1. Summary of the Advancing Contact Angle (θ_a) and Associated Hysteresis ($\Delta\theta$) Made with H_2O and Hexadecane (HD) on ODT SAMs on GaAs Surfaces (all angles are in degrees)

GaAs crystal face	$\theta_{a\text{-}H_2O}$	$\Delta\theta_{H_2O}$	$\theta_{a\text{-}HD}$	$\Delta\theta_{HD}$
(001)	111 ± 3	16 ± 4	43 ± 1	2 ± 1
(110)	110 ± 2	11 ± 4	42 ± 3	2 ± 2
(111-A)-Ga	107 ± 4	20 ± 6	43 ± 3	5 ± 4
(111-B)-As	111 ± 2	15 ± 5	39 ± 3	5 ± 3

RESULTS

Wettability of ODT SAMs on GaAs(110), (111-A)-Ga, and (111-B)-As. Sessile drop measurements of ODT SAMs on the GaAs surfaces were made with H_2O and hexadecane (HD) probe liquids. The advancing contact angle measurements (θ_a) and associated hysteresis values ($\Delta\theta$) of these drops are summarized in Table 1.

The contact angle measurements for the ODT SAMs on GaAs(110) and (111-B)-As surfaces are, within error, the same as the contact angle measurements made for ODT SAMs on GaAs(001) surfaces.[62] For ODT SAMs formed on GaAs(111)-Ga surfaces, the θ_a and $\Delta\theta$ values are much different from the ODT SAMs on either GaAs(001), (110), and (111-A)-Ga surfaces. In fact, the wettability of the ODT SAMs on GaAs(111)-Ga surfaces by water is similar to that of dodecanethiolate [$CH_3(CH_2)_{11}S$-, DDT] SAMs on GaAs(001) surfaces, which have been shown to be more disordered and less densely packed than the corresponding ODT SAMs.[52] In comparison, it is noted that the hexadecane wettability of ODT SAMs on GaAs(111-A)-Ga is nearly the same as the ODT SAMs formed on GaAs(110), (001), and (111)-As.

Surface Chemical Bonding and Monolayer Packing Density from HRXPS. ***As 3d and Ga 3d Spectra.*** The As 3d and Ga 3d HRXPS spectra (Figure 1) were taken at a photon energy of 130 eV for maximum surface sensitivity (the electron mean free path is a minimum at 50−100 eV KE),[80,81] but additional spectra also were obtained at several other photon energies. In order to view the underlying trends in detail, the spectra were decomposed into individual components and fitted self-consistently by a series of doublets with the fitting parameters chosen using the full set of spectra from all of the different photon energies. The results of the previous work on the GaAs-based SAMs[38,62] were taken into account to help verify the fitting parameters. The As 3d region was fit with three doublets assigned to bulk GaAs (~41.1 eV), elementary arsenic (As^0, ~41.8 eV), and As−S bond (~42.35 eV), along with a broad peak at high BE related to As oxides (Figure 1, unshaded). The Ga 3d re-

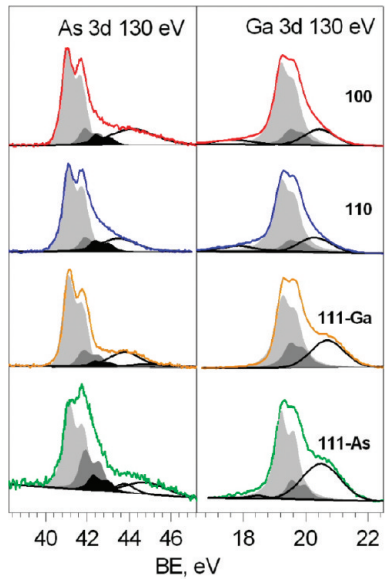

Figure 1. Ga 3d (130 eV) and As 3d (130 eV) HRXPS spectra of ODT SAMs on the GaAs(001), (110), (111-A)-Ga, and (111-B)-As faces. A decomposition of the spectral features by doublets related to individual chemical species is shown. As 3d spectra: GaAs (light gray), elementary As (gray), S−As (black), As oxides (unshaded). Ga 3d spectra: GaAs (light gray), a Ga oxide or the surface Ga 3d component (gray), Ga oxides (unshaded).

gion was fit with two doublets assigned to bulk GaAs (~19.2 eV), gallium oxide, or a surface Ga 3d component (~19.5 eV), along with a broad peak at high BE related to further Ga oxides (Figure 1, unshaded). Note that the above BEs correspond to either the As $3d_{5/2}$ or Ga $3d_{5/2}$ component.

The oxide-related features show that only minor amounts of surface oxide exist on the SAMs on the (100) and (110) faces, whereas more appears on the (111) faces. Note that because of the ambiguity in the assignment of the Ga 3d feature at ~19.5 eV, which can represent both oxide and surface Ga^0 species, the actual oxide content can be better monitored on the basis of the As 3d spectra. Most of the native oxides on bare GaAs(001) surfaces can be removed transiently by wet chemical etching[38] (see also Supporting Information) but reappear upon standing in air, which is typical for a nonprotected GaAs surface.[82] This same trend was observed for the bare (110), (111-A)-Ga, and (111-B)-As surfaces.[83] Thus the ODT molecules retard oxidation of the underlying GaAs substrate for all faces, though judging from the group of spectra, the effect appears to be greater for the square lattice (001) and (110) surfaces compared to the hexagonal (111-A)-Ga and (111-B)-As ones.

Of particular interest with respect to the adsorbate−substrate bonding is the observation that the As 3d doublet assigned to As−S bonding is considerably weaker for ODT/(111-A)-Ga than for the (100), (110), and (111-B)-As substrates. This difference also can be seen directly in the overall spectral envelopes, emphasized by the different slopes of the high BE side of the major two-peak feature. This infers that As−S bonding dominates on the (100), (110), and (111-B)-As substrates, whereas Ga−S bonding dominates on the (111-A)-Ga face. With this in mind, one would expect the appearance of a Ga−S doublet in the Ga 3d spectra but the spectra are difficult to fit in this BE region because of the close proximity of the peak at 19.5 eV.[38]

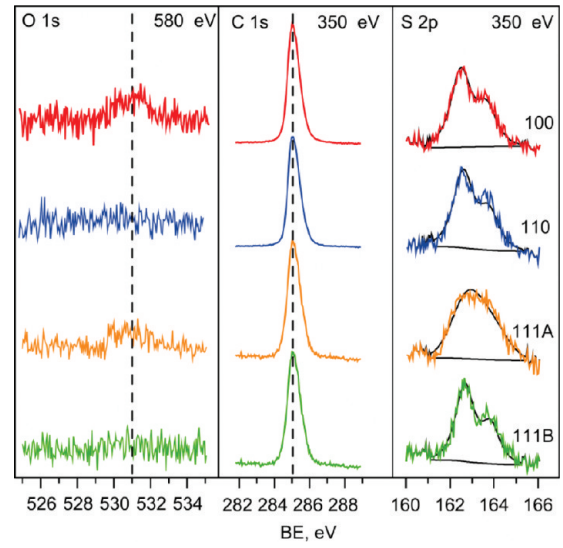

Figure 2. O 1s (580 eV), C 1s (350 eV), and S 2p (350 eV) HRXPS spectra of the ODT SAMs on GaAs(100), (110), (111-A)-Ga, and (111-B)-As surfaces (top to bottom).

S 2p Spectra. Examination of the S 2p spectra in Figure 2 shows that for all four faces a single doublet at 162.5 eV (S $2p_{3/2}$) is observed, coinciding with the previously reported value for ODT/GaAs(001) surfaces.[38] The overall spectral shape of the S 2p spectra of ODT/GaAs(111-A)-Ga is distinctly different, however, compared to the other three surfaces. Consistent with the As 3d and Ga 3d spectra, we interpret these observations in terms of dominant Ga−S bonding on the (111-A)-Ga substrate in contrast to dominant As−S boding on the (111-B)-As, (110), and (001) faces. In general, the S 2p features are not sufficiently well-resolved to be able to quantitate the fractional binding, so one can conclude that in all cases both types of bonding may exist but one or the other is dominant. Note, however, that there is a noticeable difference in the effective width of the S $2p_{3/2,1/2}$ components for the (111-A)-Ga SAM, for which these components cannot be resolved, compared to the three other surfaces, for which these components can be clearly resolved (*cf.* Figure 2). This suggests a higher structural inhomogeneity for the (111-A)-Ga SAM.

C 1s and O 1s Spectra. On all four surfaces, the BE positions of the C 1s peaks are similar (Figure 2). Note, however, that the slightly weaker C 1s signal with a slightly broader fwhm of ~0.86 eV for the (111-A)-Ga SAM compared to the three other surfaces, which exhibit almost identical fwhm values of ~0.77 eV, suggests a lower packing density and higher structural inhomogeneity

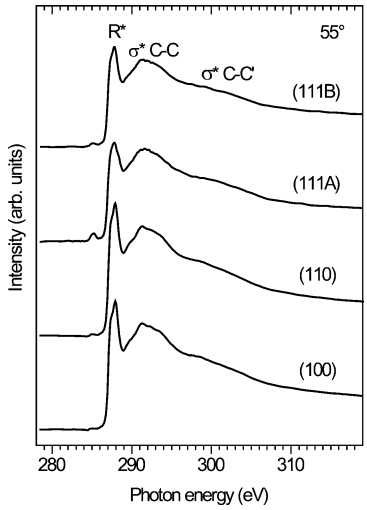

Figure 3. C *K*-edge NEXAFS spectra of ODT SAMs on the four GaAs crystal surfaces acquired at an X-ray incidence angle of 55°. The characteristic absorption resonances are marked.

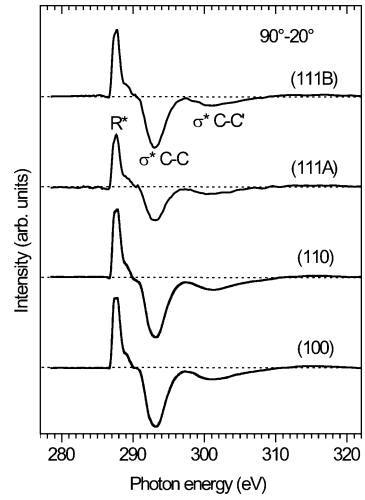

Figure 4. Difference between the C *K*-edge spectra of ODT SAMs on the four different GaAs surfaces acquired at X-ray incidence angles of 90 and 20°. The dashed lines correspond to zero. The characteristic absorption resonances are marked.

for the (111-A)-Ga SAM. This can be attributed to the shift in dominant adsorbate−substrate bonding from As−S to and Ga−S with the suggestion that the SAMs do not form as well with Ga−S bonding. For all faces, the O 1s signals are quite weak, consistent with the conclusions of only trace substrate oxidation from the Ga 3d and As 3d spectra.

Overall Conclusions from the HRXPS Spectra. The main points from the HRXPS spectra are that the presence of the ODT SAMs retards oxidation of the underlying GaAs substrate for all faces but the (111) faces appear to be more susceptible to slow oxidation. Most importantly, the data show that the dominant surface bonding shifts from As−S on the (100), (110), and (111-B)-As faces to Ga−S on the (111-A)-Ga face and that the SAMs do not organize as well on the latter surface as on the former ones.

Molecular Orientation from NEXAFS Carbon *K*-Edge Spectra.

Conformational Order and Molecular Orientation. Following the methods previously developed for utilizing NEXAFS for determining the average orientational configuration of the SAM molecules on GaAs substrates,[62] spectra were obtained at different X-ray beam angles and the data interpreted in terms of a linear dichroism analysis. In brief, the absorption resonance intensity is plotted against the angle of incidence of the impinging X-ray beam and the data analyzed in terms of the direction of the electric field vector with respect to the transition dipole moment (TDM) direction of the molecular orbital resonance of interest. Since at a 55° incidence angle (∼*magic* angle) the sample appears isotropic, these spectra serve as a convenient reference for absorption resonance assignments.[84] As seen in Figure 3, the general carbon *K*-edge resonance features of all four ODT SAMs are quite similar. The spectra exhibit (1) a C 1s absorption edge related to C 1s → continuum excitations; (2) 287.7 (*R**), ∼293.4 and ∼301.6 eV resonances characteristic of extended, *all-trans* alkyl chains. The latter three resonances are attributed to mixed valence/Rydberg states[85−87] with a dominance of Rydberg states,[88,89] valence, antibonding C−C σ* and valence, antibonding C−C′ σ* orbitals, respectively.[84,90] The sharp leading edge *R** feature shows that the alkyl chains have high conformational order.

The variable angle difference (90−20°) spectra (Figure 4) reveal significant linear dichroism, which is interpreted based on the previous assignments of the *R** and the C−C σ* and C−C′ σ* TDM orientations as perpendicular and parallel, respectively, to the long axis of the alkyl chains.[90−92] The main analysis focuses on the intense *R** resonance involving a plane-type orbital with the characteristic intensity dependence given by:[84]

$$I(\gamma,\theta) = A\left\{P \times \frac{2}{3}\left[1 - \frac{1}{4}(3\cos^2\theta - 1)(3\cos^2\gamma - 1)\right] + (1 - P) \times \frac{1}{2}(1 + \cos^2\gamma)\right\} \quad (1)$$

where *A* is a constant, *P* is a polarization factor of the X-rays, and γ is the angle between the sample normal and the normal of the molecular orbital plane. To avoid normalization problems, the intensity ratios $I(\theta)/I(90°)$, $I(\theta)/I(55°)$, and $I(\theta)/I(20°)$ were analyzed,[84] where $I(\theta)$, $I(90°)$, $I(55°)$, and $I(20°)$ are the intensities of the *R** resonance at X-ray incidence angles of 90, 55, and 20°, respectively. As an example, the $I(\theta)/I(90°)$ intensity ratios for the ODT SAMs on the four different GaAs crystal faces are presented in Figure 5, along with the respective best fits according to eq 1. Significantly, these dependences are quite similar for the (100), (110), and (111-B)-As faces but distinctly different for the (111-A)-Ga surface. The values of the average tilt angles of the alkyl chains derived from the angular data are compiled in Table 2.

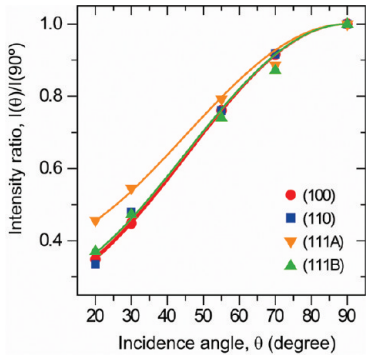

Figure 5. Angular dependencies of the *R resonance intensity ratio $I(\theta)/I(90°)$ for the ODT SAMs on the (100), (110), (111-A), and (111-B) GaAs crystal faces (red circles, blue squares, yellow triangles, and green triangles, respectively), along with the respective best fits according to eq 1 marked by the solid lines.**

In addition to the above standard evaluation procedure, we processed the NEXAFS data using the difference spectra, which were calculated similar to the 90−20° spectra presented in Figure 4. According to previous work,[84] upon subtracting two NEXAFS spectra recorded at different X-ray incidence angles θ and θ_1, one obtains

$$I_v(\theta) - I_v(\theta_1) = C_v\left(1 - \frac{3}{2}\sin^2\alpha\right)(\cos^2\theta - \cos^2\theta_1) \quad (2)$$

$$I_p(\theta) - I_p(\theta_1) = C_p(1 - 3\cos^2\gamma)(\cos^2\theta - \cos^2\theta_1) \quad (3)$$

for a vector (v) and a plane (p) and orbital, respectively. $I_{v/p}(\theta)$ and $I_{v/p}(\theta_1)$ are the resonance intensities, α is the angle between the sample normal and the TDM of the vector orbital, γ was described above, and $C_{v/p}$ is a normalization constant, which depends on the excitation probability from the C 1s core level into a given molecular orbital. Following eqs 2 and 3, we plotted the intensities of the difference peaks for the *R** and σ* C−C resonances *versus* $\cos^2\theta - \cos^2 20°$ for ODT SAMs on the four different GaAs surfaces in Figure 6, along with the corresponding data set for HDT/Au. The slopes of the lines, which are quite similar for the (100), (110), and (111-B)-As faces but distinctly different for the (111-A)-Ga surface, give us $C_p(1 - 3\cos^2\gamma)$ and $C_v(1 - {}^3/_2\sin^2\alpha)$ for the *R** and σ* C−C resonances, respectively. Then, assuming the average tilt angle of the alkyl chains in HDT/Au to be 30°, in accordance with our own results and literature data,[84,90−92] we calculate C_v and C_p and get the average tilt angle of the alkyl chains in ODT SAMs on the four different GaAs surfaces. The respective data are included in Table 2.

TABLE 2. Molecular Tilt Angles of ODT Self-Assembled Monolayers on the GaAs(100), GaAs(110), GaAs(111-A)-Ga, and GaAs(111-B)-As Surfaces Derived from the C *K*-Edge NEXAFS and IR Spectra[a]

	tilt angles of ODT on GaAs Crystal Faces (degrees)			
C 1s resonance:	(100)	(110)	(111-A)-Ga	(111-B)-As
*R**, absolute intensity	18.0	17.8	28.0	19.0
*R**, difference	16.4	17.5	26.3	17.9
σ* C−C, difference	15.8	17.2	29.1	16.4
C 1s average value	16.7(±0.8)	17.5(±0.2)	27.8(±1.3)	17.7(±0.9)
IRS	15(±1.5)	18(±1.5)	<30	20(±1.5)

[a]The NEXAFS tilt angles derived from three different methods and the average tilt angle from these methods are reported.

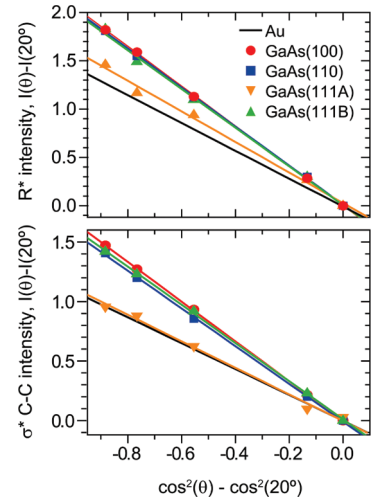

Figure 6. Plots of the intensities of the *R (top panel) and σ* C−C (bottom panel) difference peaks for ODT assembled on the four (100), (110), (111-A), and (111-B) GaAs crystal faces and HDT assembled on Au{111} *versus* $\cos^2\theta - \cos^2 20°$ along with the respective linear fits using least-squares analysis. The derived average alkyl chain tilt angles are summarized in Table 2. The data for HDT assembled on Au{111} are reported for comparison.**

Overall, the NEXAFS results of sharp *R** resonances provide qualitative evidence that the SAMs are in general well-organized with extended alkyl chains in dominant highly *trans* conformations. The angle-dependent data of the resonances give chain tilt angle values (Table 2) of ~17° for the (100), (110), and (111-B)-As faces but comparably larger (~28°) for the ODT SAM on the (111-A)-Ga substrate.

Chain Conformational Ordering and Orientation from IRS C−H Stretching Mode Frequencies. ***Chain Conformational Ordering.*** Changes in the C−H stretching mode peaks provide a qualitative measure of the chain conformational order of each SAM and have been analyzed previously for the ODT SAM on GaAs(001).[62] For ODT SAMS on the (110) and (111-B)-As index GaAs surfaces, these modes appear at the same frequencies as the ODT SAMS on GaAs(001), 2850 cm^{-1} [$-CH_2-$ sym str (d^+)], 2878 cm^{-1} [CH_3 sym str (r^+) split by Fermi resonance (FR) interaction with the CH_3 asym def], 2917 cm^{-1} [$-CH_2-$ antisym str (d^-)], and 2967 cm^{-1} [CH_3 asym in-plane str (r_a^-)] (see Figure 7). For ODT SAMS on the (111-A)-Ga surface, both the d^+ and d mode peaks shift relatively to higher frequencies (~2719−2720), but most notably, the intensities are significantly decreased and the peaks broadened, indicative of a decrease in the chain conformational ordering. The spectrum is quite similar to that

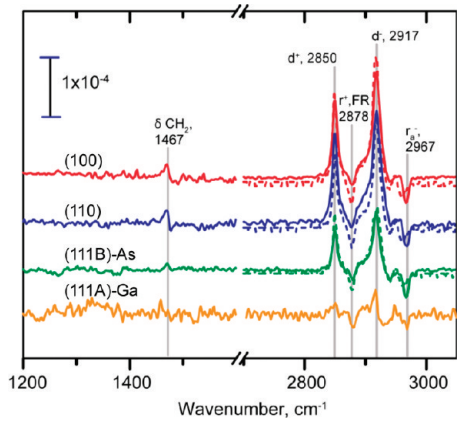

Figure 7. IRS spectrum of ODT molecules assembled on the four low-index GaAs surfaces. Vertical lines are drawn as a guide to the eye to show the shift in peak position (cm^{-1}). Simulated IRS spectra using a two-chain per unit cell model with chains in an all-*trans* configuration (dotted lines) are included for comparison for the high-frequency C−H stretching region. Simulations were not performed for the (111-A)-Ga SAM spectrum because the spectral features were associated with significant alkyl chain disorder.

for the dodecanethiol on GaAs(001) SAM, which is observed to have poor organization with no evidence of translational ordering.[52]

In the low-frequency region of the p-polarized spectrum (Figure 7), the 1467 cm^{-1} peak is assigned to the CH_2 scissor deformation mode (δ CH_2). No obvious splitting is seen within the resolution and signal/noise of our spectra. Splitting has been noted to occur in this mode for close-packed polymethylene chains in a two-chain/unit subcell in an orthorhombic packing crystal structure.[93] While this type of structure arises in alkanethiolate/Au{111} SAMs,[59] well-defined splitting of this mode has been observed only at low temperatures (*e.g.*, for the $C_{22}H_{45}S$-/Au{111} SAM).[94]

Chain Orientation. For all ODT SAMs formed on the four low-index GaAs surfaces, the d^+ and d^- modes have positive absorbance features similar to the features observed for ODT SAMs on GaAs(001) (Figure 7). It has been previously established for this SAM through analysis of the IRS r_a^- mode intensities that the molecules adopt a two-chain/unit cell structure. Accordingly, simulations of the spectra of the ODT SAMs on the (110) and (111-B)-As surfaces were carried out for an air/SAM/GaAs sample with fully extended, oriented chains in a two-chain/unit cell structure. The SAM layer thickness was set at the NEXAFS derived values of 23.5(±0.3), 23.2(±0.3), and 22.9(±0.3) Å for the (001), (110), and (111-B)-As surfaces, respectively, and a single set of values of the refractive index dispersion with frequency was used for GaAs. In the two-chain model, the final spectra were calculated as 1/2(S1 + S2), where S1 and S2 are the two individual spectra.

The previously determined best fit for the ODT/GaAs(001) system (shown in the figure for comparison) corresponded to a chain tilt, $\Phi = -15(\pm 1.5)°$, and twists, $\Psi = 43°,133°$ (both ±10°), consistent with a herringbone packing and 90° setting angle between the C−C−C planes.[52] For the ODT/(110) and (111-B)-As SAMs, best fits were obtained with chain tilts $\Phi = -18$ and −20° (both ±1.5°) and twists $\Psi = 43°,133°$ and $\Psi = 43°,133°$ (all ±10°), respectively, in excellent agreement with the NEXAFS data, showing the self-consistency of the film thickness and chain orientation values. The results for all of the best fit chain tilt angles are summarized in Table 2.

For the ODT/GaAs(111-A)-Ga SAM, a singular best fit with simulations assuming fully extended all-*trans* chains could not be determined. A range of chain tilts, $\Phi = 25-30°$, and twists, $\Psi = 40-45°$, were found to have similar fits to the data. Since tilt angles >30° result in negative intensities for the d^+ and d^- modes,[62] a limit of a 30° molecular tilt angle was imposed. The inability to fit the ODT/GaAs (111-A)-Ga spectra to an ideal all-*trans* two-chain model is consistent with the considerable conformational disorder.

Translational Ordering from GIXRD. ***Summary of GIXRD of ODT SAMs on GaAs(001).*** Previously,[52] GIXRD data for the ODT SAMs on GaAs(001) surfaces were shown to have distinct translational ordering of the adsorbate. Analysis of the Bragg reflections observed at slightly off ~30 and/or ~60° intervals led to the derivation of a pseudohexagonal unit cell exhibiting NN spacings of 4.70 and 5.02 Å, domain sizes of ~66−74 Å, and packing densities of 21.2 $Å^2$/molecule. These results are used for comparison for the ODT SAMs adsorbed on the GaAs(110), (111-B)-As, and (111-A)-Ga surfaces.

GIXRD of the ODT SAMs on GaAs(110). Bragg reflection scans on independently prepared ODT SAM samples on GaAs(110) revealed Bragg reflection patterns with peak intensities showed maxima at nominal 60° azimuthal separations, an indication of preferential orientation of the thiol domains along hexagonal symmetry. With the azimuthal angle ϕ set to zero for the GaAs[100] reference direction (see Figure 8C), two of the reflections were observed at 1° off the [100] direction ($\phi = 1°$) and 58° off the [100] direction ($\phi = 58°$), corresponding to $q_{xy} = 1.48$ $Å^{-1}$ (Figure 8A) and $q_{xy} = 1.51$ $Å^{-1}$ (Figure 8B), seen in the radial maps, respectively. A third peak was also observed at −63° off the [100] direction ($\phi = -63°$) corresponding to $q_{xy} = 1.51$ $Å^{-1}$.[95] The observed radial fwhm (Δ) of 0.10 $Å^{-1}$ for the three peaks yields an average domain size of ~70 Å.[96] The existence of two slightly different q_{xy} values and the deviations from exact 60° azimuthal peak separations (see Table 3) indicate a distorted or pseudohexagonal structure and is similar to the same structural trend observed for the ODT SAMs on GaAs(001) surfaces.

Azimuthal rotation of the sample around each Bragg reflection peak setting showed an azimuthal width $\Delta\phi$ with a fwhm of ~25°. This value represents the orientational inhomogeneity of monolayer domains across the surface. In the case of a perfect powder, no independent azimuthal peaks would be observed; instead,

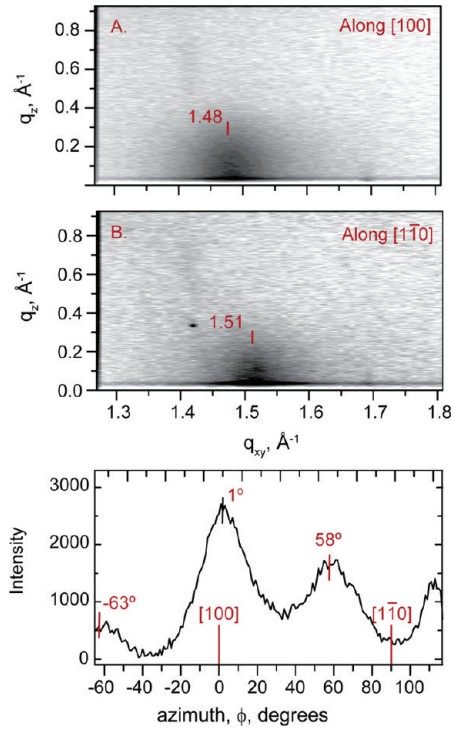

Figure 8. X-ray diffraction through the first-order diffraction peaks of the ODT monolayers GaAs(110) as a function of q_{xy}. (A) Radial map along the [001] direction; the monolayer reflection is observed at $q_{xy} = 1.48$ Å^{-1}. (B) Radial map along the [1−10] direction; the monolayer reflection is observed at $q_{xy} = 1.51$ Å^{-1}. (C) Azimuthal orientation (ϕ) of the ODT monolayer reflections with $\delta\phi \sim 60°$. The position of the [100] substrate directions is marked with a vertical line. The monolayer reflections are observed 1, 58, and −63° off the GaAs[001] direction ($\phi = 0°$).

the azimuthal scan would show a constant intensity corresponding to a homogeneous in-plane powder ring. This result shows that there is only a weak azimuthal alignment of the thiol domains on GaAs compared to other SAM systems, for example, alkanethiolate domains on Au(111), but is consistent with the degree of orientation observed for ODT SAMS on GaAs(001) surfaces. However, this weak alignment of the ODT SAMs along the [001] direction of the GaAs(110) substrate is the same direction DDT SAMs were observed to orient on InP(110) surfaces.[77−79]

Analysis of the radial peak position along specific azimuths yields two different nearest neighbor (NN) distances, 4.83 Å along the $\phi = 27°$ (90 + −63°) and the $\phi = 91°$ (90 + 1°) directions and 5.10 Å along the $\phi = 148°$ (90 + 58°) direction. These NN distances and their azimuthal separations ($\delta\phi$, see Table 3) lead to a reciprocal areal density of ∼21.3 Å^2/molecule, approximately the same density as the reciprocal areal density reported for ODT SAMS on GaAs(001) surfaces. The azimuthal texture of the monolayer in-plane powder ring is similar to what has been observed for these SAMs by LFM, but the inter-row spacings are smaller than the 5.7 Å spacings observed previously.[74]

Figure 9 depicts the proposed lattice structure superimposed on an ideal unreconstructed, GaAs(110) surface with the [001] direction indicated for reference. The schematic incorporates the two-chain per unit cell herringbone structure as predicted by the IRS spectra. A representation of the pseudohexagonal unit subcell is also shown. Note that none of the NN distances of the SAM monolayer structure correspond within errors to the NN (2.450, 3.995) or NNN (4.680 Å) distances of the intrinsic GaAs(110) rectangular lattice plane, and thus the hexagonal monolayer is highly incommensurate with the intrinsic substrate surface lattice, but there are preferable lattice matches in one direction.[16] Given the preferential alignment of the adsorbate molecules along the [100] direction, the Bragg reflections and their azimuthal orientation were used to construct the reciprocal space unit cell and the real space orientation of the monolayer with respect to an ideally terminated (110) GaAs surface and are shown in Figure 9. Although the exact termination and reconstruction of the (110) surface is not known, it can be inferred from these representations that the incommensurate pseudohexagonal structure of the ODT SAMs results from the monolayers trying to accommodate specific binding sites on the (110) surface.

TABLE 3. Summary of the Bragg Reflection Data for the ODT SAMs on GaAs(110), (111-B)-As, and (111-A)-Ga and *epi*-GaAs(001)

GaAs surface	Bragg reflection position (Å^{-1})	fwhm Δq_{xy} (Å^{-1})	domain size (Å)	azimuthal positions of Bragg reflections (degrees)	azimuthal separation between specific Bragg reflections ($\delta\phi$) (degrees)
(100)[52]	1.49	0.08	∼70	$\phi_A{}^a = 64$	$\delta\phi_{AB} = 67$
	1.51	0.09		$\phi_A{}^a = -51$	$\delta\phi_{BC} = 53$
				$\phi_A{}^a = 1$	$\delta\phi_{CA} = 60$
(110)	1.48	0.12	∼70	$\phi_A{}^b = 1$	$\delta\phi_{AB} = 57$
	1.51	0.11	∼70	$\phi_B{}^b = 58$	$\delta\phi_{BC} = 59$
				$\phi_C{}^b = -63$	$\delta\phi_{CA} = 64$
(111-B)-As	1.48	0.11	∼70	$\phi_A{}^c = -3$	$\delta\phi = 60$
(111-A)-Ga	1.48	0.16	∼70	$\phi_A{}^c = 60$	$\delta\phi = 60$

[a]Values are with respect to $\phi = 0°$ for the [100] direction on the GaAs(110) surface. [b]Values are with respect to $\phi = 0°$ for the [110] directions on the GaAs(111) surfaces and were fit to a certainty of 0.1−0.7°, depending on each individual sample.

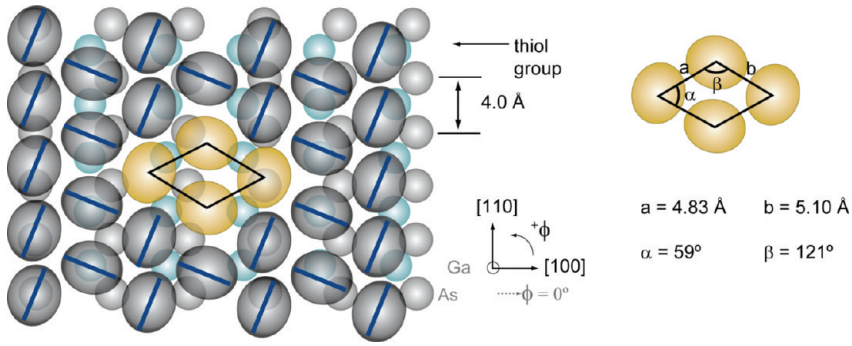

Figure 9. (Left) Molecular unit cell embedded in a larger, ideal monolayer overlayer structure. The monolayer structure is shown in real space with respect to an ideal intrinsic As-terminated (110) GaAs surface. The gray ellipses represent top-down vertical projections of untilted thiolate chains onto the substrate plane with the C−C−C planes indicated as blue bars. The relative twists of the chains show the herringbone pattern deduced from the IRS data. (Right) Representation of a unit subcell and the associated lattice parameters.

GIXRD of the ODT SAMs on GaAs(111-B)-As and GaAs(111-A)-Ga Surfaces. Bragg reflection scans on independently prepared ODT SAMs on GaAs(111-B)-As samples revealed that Bragg reflection patterns with peak intensities showed maxima at nominal 60° azimuthal separations, an indication of preferential orientation of the thiol domains along hexagonal symmetry. With the azimuthal angle ϕ set to zero for the GaAs [1$\bar{1}$0] reference direction (see Figure 10), two of the reflections were observed at 3° off the [1$\bar{1}$0] direction ($\phi = -3°$) and 57° off the [1$\bar{1}$0] direction ($\phi = -57°$), corresponding to $q_{xy} = 1.48$ Å^{-1} (Figure 10). The observed radial fwhm (Δ) of 0.11 Å^{-1} for the peaks yields an average domain size of ~70 Å.[96] Unlike the rectangular GaAs(001) and (110) surfaces, on the hexagonal (111-B)-As surface, only one q_{xy} value was observed. Furthermore, since the azimuthal peak separations are 60° apart, this indicates that the SAMs organize in an undistorted hexagonal structure.

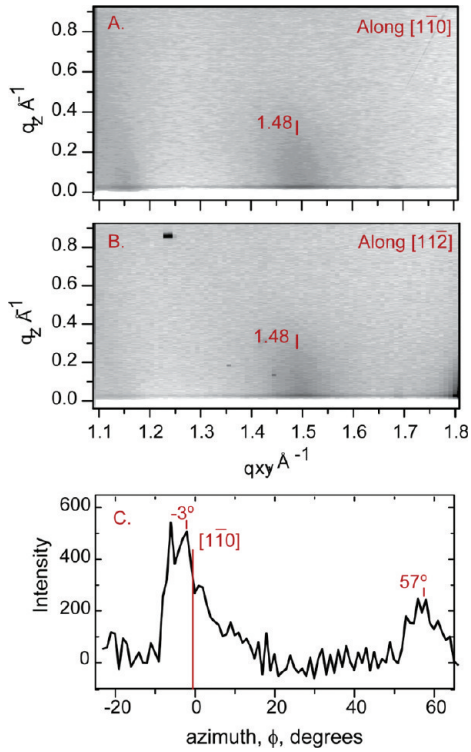

Figure 10. X-ray diffraction through the first-order diffraction peaks of the ODT monolayers GaAs(111-B)-As as a function of q_{xy}. (A) Radial map along the [1$\bar{1}$0] direction; the monolayer reflection is observed at $q_{xy} = 1.48$ Å^{-1}. (B) Radial map along the [11$\bar{2}$] direction; the monolayer reflection is observed at $q_{xy} = 1.48$ Å^{-1}. (C) Azimuthal orientation (ϕ) of the ODT monolayer reflections with $\delta\phi = 60°$. The position of the [120] substrate directions is marked with a vertical line. The monolayer reflections are observed −3 and 57° off the [1$\bar{1}$0] direction ($\phi = 0°$), corresponding to $\delta\phi = 60°$.

Analysis of the $\delta\phi = 60°$ azimuthal dependence yields one nearest neighbor (NN) distance, 4.90 Å. This NN distance and its azimuthal separations ($\delta\phi$, see Table 3) lead to a reciprocal areal density of ~20.8 Å^2/molecule, slightly less dense than the reciprocal areal density reported for ODT SAMS on GaAs(001) and (110) surfaces.

Figure 11 depicts the proposed lattice structure superimposed on an ideal unreconstructed, As-terminated GaAs(111) surface with the [1$\bar{1}$0] direction indicated for reference. The schematic incorporates the two-chain per unit cell herringbone structure as predicted by the IRS spectra. A representation of the hexagonal unit subcell is also shown. Note that none of the NN distances of the SAM monolayer structure correspond within errors to the NN distance (3.995 Å) of the intrinsic GaAs(111) hexagonal lattice plane, and thus the monolayer is highly incommensurate with the intrinsic substrate surface lattice. Note also, however, this incommensurate structure does not lead to the observation of homogeneous powder rings in the azimuthal scans. Rather, the distinct presence of azimuthal peaks (width of ~10°) indicates a preferred order of the thiolate molecules on the surface. The Bragg reflections and their azimuthal orientation were used to construct the reciprocal space unit cell and the real space orientation of the monolayer with respect to an ideal As-terminated (111) GaAs surface and are shown in Figure 11.

On the GaAs(111-A)-Ga surface, a similar superlattice structure of the ODT SAMs on the GaAs(111-B)-As

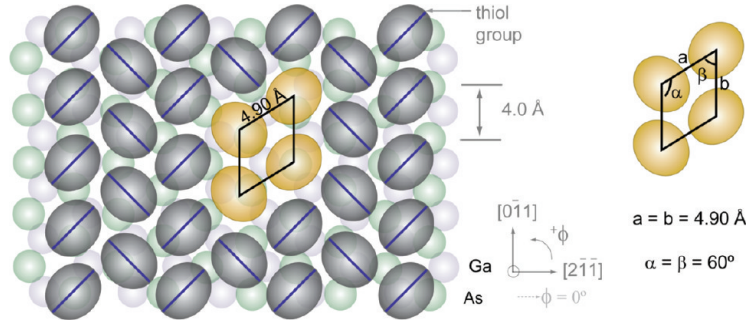

Figure 11. (Left) Molecular unit cell embedded in a larger, ideal monolayer overlayer structure. The monolayer structure is shown in real space with respect to an ideal intrinsic As-terminated (111-B) GaAs surface. The gray ellipses represent top-down vertical projections of untilted thiolate chains onto the substrate plane with the C−C−C planes indicated as blue bars. The relative twists of the chains show the herringbone pattern deduced from the IRS data. (Right) Representation of a unit subcell and the associated lattice parameters.

surface was observed. With the azimuthal angle ϕ set to zero for the GaAs [1$\bar{1}$0] reference direction (see Figure 12), reflections were observed at 60° off the [1$\bar{1}$0] direction ($\phi = 60°$). Like the GaAs(111-B)-As surface, only diffraction spacing corresponding to $q_{xy} = 1.48$ Å^{-1} was observed from the ODT monolayers on this surface. From the fit of the integrated intensity of the diffraction peak, a peak width $\Delta q_{xy} = 0.16$ Å^{-1} was determined, corresponding to a domain size of ~70 Å. Analysis of the $\delta\phi = 60°$ azimuthal dependence yields one nearest neighbor (NN) distance, 4.90 Å, with a reciprocal areal density of ~20.8 Å^2/molecule, similar to the (111-B)-As surface.

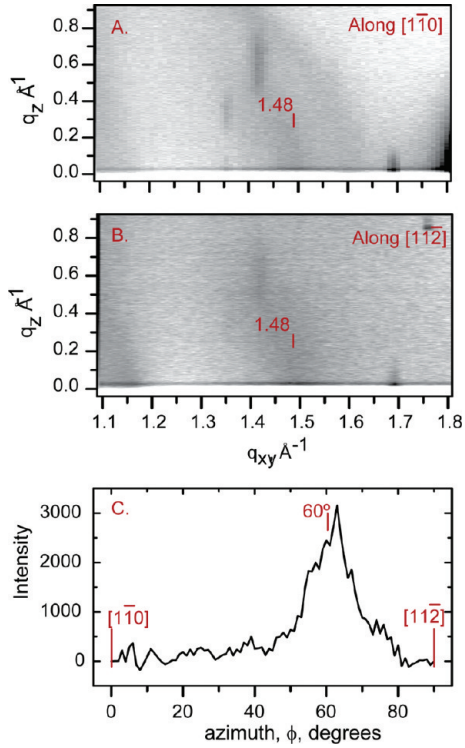

Figure 12. X-ray diffraction through the first-order diffraction peaks of the ODT monolayers of GaAs(111-A)-Ga as a function of q_{xy}. (A) Radial map along the [1$\bar{1}$0] direction; the monolayer reflection is observed at $q_{xy} = 1.48$ Å^{-1}. (B) Radial map along the [11$\bar{2}$] direction; the monolayer reflection is observed at $q_{xy} = 1.48$ Å^{-1}. (C) Azimuthal orientation (ϕ) of the ODT monolayer reflections with $\delta\phi = 60°$. The positions of the [1$\bar{1}$0] and [11$\bar{2}$] substrate directions are marked with a vertical line. The monolayer reflections are observed 60° off the [1$\bar{1}$0] direction ($\phi = 0°$), corresponding to $\delta\phi = 60°$.

Unlike the diffraction peaks of the ODT SAMs on the (001), (110), and (111-B) surfaces, the diffraction peaks on the (111-A)-Ga surface have faintly associated powder rings. This indicates that there is no azimuthal alignment of the thiol domains on the (111-A)-Ga surface compared to other GaAs SAM systems. Additional, in-plane, sharp ($\Delta q_{xy} \sim 0.01$ Å^{-1}) Bragg peaks at $q_{xy} = 1.39$, 1.41, and 1.68 Å^{-1} on the ODT SAMs were also observed on the radial maps of these samples (see Figure 12), even after minimal X-ray beam exposure. While these peaks are observed to grow after significant (~12−24 h) X-ray beam exposure on other well-formed ODT/GaAs systems (*i.e.*, 100, 110, and 111-B-As), the immediate appearance of these X-ray-induced monolayer structures suggests a higher susceptibility of the Ga-S bonding to x-ray damage compared to As-S bonding.

Role of Step Edges: ODT SAMs on *epi*-GaAs(001). In our previous report,[52] we noted that on the basis of GIXRD data ODT SAM formation on the surface of a GaAs(001) single crystal shows a strong tendency for the SAM domains to align along the substrate [1$\bar{1}$0] crystal directions. This observation was concluded to be consistent with a transitioning assembly mechanism in which the initial adsorbate thiols chemisorb at [1$\bar{1}$0] step edges in preference to the lower energy (001) surface plane and then subsequently seed domain growth across the (001) plane such that the emerging strong intermolecular packing forces dominate the overall SAM energetics and force substrate terrace atom restructuring. In order to test this conclusion, further experiments were done with *epi*-GaAs(001) substrates which contain no inherent step edges.

The results of liquid drop contact angle, quantitative IRS, and XPS measurements for the *epi*-GaAs(001) ODT SAMs show complete agreement with our earlier results on the standard single-crystal (001) surfaces containing step edges (data are given in the Supporting Information). Since these characterizations would not be

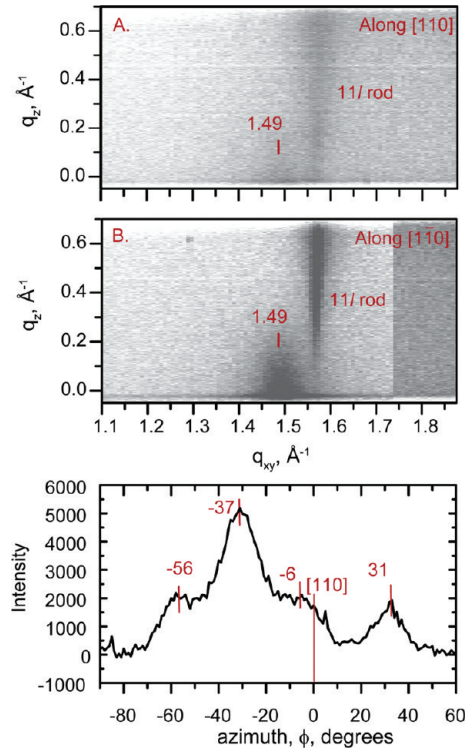

Figure 13. X-ray diffraction through the first-order diffraction peaks of the ODT monolayers on *epi*-GaAs(001) as a function of q_{xy}. (A) Radial map along the [110] direction; the monolayer reflection is observed at q_{xy} = 1.49 Å^{-1}. (B) Radial map along the [1$\bar{1}$0] direction; the monolayer reflection is observed at q_{xy} = 1.49 Å^{-1}. In both scans, a sharp 11*l* rod is observed, indicative of a well-ordered GaAs(001) surface. (C) Azimuthal orientation (ϕ) of the ODT monolayer reflections with $\delta\phi \sim 30°$. The position of the [110] substrate directions is marked with a vertical line. The monolayer reflections are observed −6, −37, −56, and 31° off the [100] direction (ϕ = 0°).

expected to reflect subtle effects of occasional step edges on the surface, the agreement indicates that the same overall molecular packing is obtained on both the epitaxial and the standard crystal (001) surfaces.

GIXRD measurements, on the other hand, will be sensitive to step edge effects on the lateral organization of the ODT molecules. The surface corrugation on a perfect GaAs(001) surface can give rise to preferential orientations of the thiol hexagons.[16] If the hexagons are lined up with the equivalent [100] and [010] (or alternatively [110] and [1$\bar{1}$0]), there would be maxima separated by 30°. With the azimuthal angle ϕ set to zero for the GaAs[110] reference direction (see Figure 13C), diffraction scans on independently prepared ODT SAM samples on *epi*-GaAs(001) revealed reflections at −56,−37, −6, and 31° off the [110] direction (ϕ = 0°). The corresponding q_{xy} = 1.49 Å^{-1} (Figure 13) was seen in the radial maps along the [110] and [1−10] direction of the substrate. The observed radial fwhm (Δ) of 0.11 Å^{-1} for the diffraction peaks yields again an average domain size of ~70 Å.[96] In both scans, a sharp 11*l* crystal truncation rod (CTR) of the substrate is observed, indicative of a well-ordered GaAs(001) surface. This diffraction signal is significantly different from the ODT SAMs on GaAs(001) surfaces,[52] where two different diffraction spacings were observed, but no CTR, indicating a much higher roughness. Here, the diffraction spacing of q_{xy} =1.49 Å^{-1} corresponds to the diffraction spacings of the ODT SAMs on GaAs(001) along the nonstep edge directions.[52] The much stronger appearance of the GaAs truncation rods suggests that the epitaxial surfaces are significantly smoother than the surfaces that resulted after wet etching the native oxide.[96]

Overall, these maxima differ by steps of ~30° and are similar to the ~30° separation observed in pattern II of the ODT SAMs on GaAs(001) surfaces. In another sample of ODT SAMs on *epi*-GaAs(001), separations of ~60° were also observed, consistent with the observation that on (001) surfaces the different azimuthal dependence of the Bragg reflections in the two monolayer structures could be due to the presence of two different SAM domain alignments differing by 30°.

It should also be noted that, like the GaAs(111-A)-Ga-terminated surfaces, the ODT molecules assembled on the epitaxial GaAs(001) surfaces were far more susceptible to beam damage. However, in the case of the epitaxial GaAs(001), as the SAMs were exposed to the X-ray over time, there was a reduction in the intensity of the diffraction pattern finally resulting in the complete absence of diffraction peaks. This is in stark contrast to the other GaAs surface faces, where prolonged exposure to the X-ray beam resulted in new, beam-induced, highly crystalline phases.

DISCUSSION

Overview Summary of the Results. In our previous report of alkanethiolate and arenethiolate SAMs on GaAs(001) surfaces, we showed the intricate balance between the molecule−substrate and intermolecular interactions in determining the final SAM structure. In that study, the balance was probed by changing the number (*i.e.*, chain length) and type (*i.e.*, van der Waals, $\pi-\pi$) of interactions between the self-assembling molecules[52] with the finding that for alkanethiolates a high degree of self-organization did not set in until ~16 C atom or greater chains. In the present study, variations in the GaAs crystal termination have been made while keeping the intermolecular interactions constant by focusing solely on the ODT adsorbate molecule with an 18 carbon alkyl chain. In this way, we could explore correlations of structure with the substrate intrinsic lattice symmetry and spacings.

A comprehensive summary of the molecular structures observed on the different GaAs termination faces, along with the intrinsic substrate lattice characteristics for reference in the discussion, is given in Table 4. There are four important points to notice.

First, the molecular lattices all exhibit a general hexagonal type of symmetry, regardless of the underlying intrinsic substrate lattice symmetry. Second, the nearest

TABLE 4. Summary of Structural Parameters for the Different SAM and Intrinsic GaAs Crystal Surfaces in This Study[a]

	GaAs(001)	GaAs(110)	GaAs(111)-As	GaAs(111)-Ga
unit mesh (GIXRD)	$a \neq b$ $a = 4.70$ Å $b = 5.02$ Å $\alpha \neq \beta$ $\alpha = 115°$ $\beta = 65°$	$a \neq b$ $a = 4.83$ Å $b = 5.10$ Å $\alpha \neq \beta$ $\alpha = 59°$ $\beta = 121°$	$a = b$ $a = 4.90$ Å $\alpha = \beta$ $\alpha = 60°$	$a = b$ $a = 4.90$ Å $\alpha = \beta$ $\alpha = 60°$
packing geometry (GIXRD)	pseudohexagonal	pseudohexagonal	hexagonal	hexagonal?[d]
intrinsic substrate lattice spacings, Å	3.995	2.450, 3.995	3.995	3.995
SAM relation to substrate (GIXRD)	*incommensurate*; aligned along [110][c]	*incommensurate*; aligned along [100][c]	*incommensurate*; aligned along [110] or between [110] and [211]	*incommensurate*; along [110] or between [110] and [211]
average SAM domain size (GIXRD), Å	~70	~70	~70	~60
SAM area (GIXRD) per molecule, Å^2	~21.2	~21.3	20.8	20.8
intrinsic area per substrate atom, Å^2	15.96	9.787	3.460	3.460
molecular tilt angle (NEXAFS, IRS), deg[b]	17	18	18	~28
2-Chain model molecular twists (IRS), deg[e]	43, 133	43, 133	43, 133	no fit obtained

[a]The intrinsic substrate lattice spacings and area per atom refer to a bare, GaAs surface with the intrinsic bulk structure. [b]Average error of ~±1°. [c]Indicates substrate step edge direction. [d]GIXRD shows a very weak monolayer signal, indicative of a poorly ordered monolayer. [e]Average error of ±10°.

neighbor adsorbate spacings are remarkably similar for all of the surfaces. Third, the specific values in each case are incommensurate with the intrinsic substrate lattice spacings, even in the cases of the hexagonal (111) substrates. In agreement with the conclusions in our previous report on the GaAs(001) SAM, these results show that the molecular organization is driven primarily by the intermolecular forces between the molecules to assemble in a hexagonal motif, such as would occur in the limit of a featureless surface, such as a liquid, but with shorter range order than can be sustained on a liquid.

In discussing the interplay of forces in driving the surface adsorbate organization, it is helpful to consider limiting cases of surface assembly, as shown in Figure 14. On a liquid surface (Figure 14, case III), the barrier for lateral translation of adsorbates is on the order of *kT* or lower, which effectively allows the intermolecular packing forces to drive the assembly to long-range order with spacings dictated by the lowest potential energy packing. Though the GaAs cases, with constant hexagonal molecular packing regardless of lattice symmetry, are reminiscent of the liquid substrate limit, it is clear that the strong substrate−molecule binding puts alkanethiolate−GaAs surface assembling more toward the limit of strong substrate bonding, such as case I (Figure 14), in which the molecules are pinned at specific substrate lattice points in deep wells with no lateral mobility to anneal, for example, the case of adsorbates bonded to Si(111) *via* covalent C−Si bonds.[14,15] Note for the intermediate case II (*e.g.*, alkanethiolates on Au(111)) the adsorbates are pinned at specific surface lattice sites with favorable spacings to allow commensurate template-coupled superlattices but with lateral mobilities sufficiently high to allow annealing for long-range adsorbate ordering.[24] We conclude from our results that the major difference from these cases is that the interatomic forces between the Ga and As atoms in the substrate are insufficient to serve as a rigid template for the SAM organization, and the substrate surface lattice undergoes some degree of compliant strain during the monolayer formation to assemble similarly to what would occur on a liquid substrate but with much shorter range order, as shown by comparing cases I-A and III in Figure 14. The differences in SAM cov-

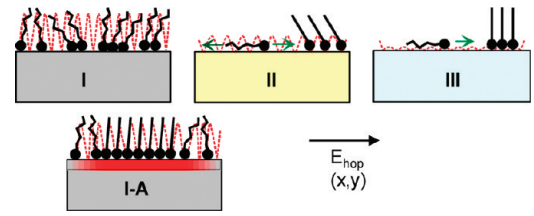

Figure 14. Schematics of three limiting cases of molecular surface self-assembly. The schematics show alkyl chain molecules pinned at substrates with varying limits of adsorbate−surface barriers for lateral translation from site to site (hopping barriers), where the hopping barriers are indicated by dashed red curves. From left to right, the hopping barriers decrease from large with deep wells to ~0. (I) Limiting case of large hopping barriers with no lateral mobility, leaving adsorbates pinned at specific lattice sites. This is the case of kinetic control of organization where the monolayer cannot anneal and any order is due to coincidental fitting of molecular sizes with lattice pinning site spacings. (II) Intermediate case in which the molecules are pinned at surface lattice sites but hopping barriers are on the order of *kT* or slightly larger, allowing annealing of the monolayer to a template-imposed superlattice. (III) Case of a featureless liquid substrate with complete lateral mobility and complete decoupling of the monolayer organization from the substrate structure. (III-A) Case of ODT on GaAs in which the adsorbates are pinned to substrate lattice atoms by strong covalent bonds but the substrate surface lattice is able to undergo strain to allow molecular packing to achieve the types of structures on a liquid substrate but with much shorter range order due to the limited ability of the GaAs substrate to compliantly strain over distances of the molecular correlation lengths (~6−7 nm). The picture shows a red region in the substrate surface layer in which compliant strain is occurring, but the strain decays at the edges to degrade further adsorbate ordering in that region.

erage and/or organization between the Ga- and As-terminated (111) surfaces would seem to indicate an inherent difference in the ability of molecular packing forces to strain the two lattices.

Finally, the average areas per molecule are significantly less than the intrinsic areas per substrate atom, an indication that a significant fraction of the substrate atoms remains unbonded to molecules in the final structures. It is likely that the atoms are instead predominantly terminated by the H atoms from the adsorbed thiol, but this issue remains in question.

Comparison of SAM Structures on Monolithic and *epi*-GaAs(001) Faces. The ODT SAM structure on a monolithic GaAs(001) surface containing dominant [110] steps was investigated previously in detail.[52] In the present study, an epitaxially grown, step-free surface has been used. Both surfaces essentially give identical SAM structures with the main exception that on the epitaxial surface the ODT domains exhibit no preference for alignment along any of the intrinsic substrate lattice directions, in contrast to the monolithic case with preferential alignment along the [110] steps. These data support our previous conclusion that the SAM domains preferentially nucleate at step edges and grow outward along the (111) terraces. In turn, this conclusion implies that the chemisorption occurs faster at the step edges, presumably because of more favorable energetics for the S−H bond dissociation.

Comparison of SAM Structures on the (001) and (110) GaAs Surfaces. The GaAs(001) and (110) substrates, which exhibit square and rectangular intrinsic lattice symmetry, respectively, both form pseudohexagonal ODT SAM structures, in accordance with the domination of intermolecular packing forces over interatomic surface lattice forces of the substrate and the formation of strong As−S surface bonding. Some insight into the overlayer structure can be gained by considering the structure of the ideal unreconstructed substrate which consists of parallel zigzag rows of alternating Ga and As atoms along the [110] direction with NN distances of 2.46 Å. This distance is far too small to accommodate rows of alkanethiolate molecules (~4.5 Å diameter), while along the [100] direction, with a 5.65 Å NN spacing, the distance is much too large to be assigned to any of the lattice spacings observed for the ODT SAMs (Table 4). A third NN distance of 4.68 Å exists 25° off the [100] direction and is approximately the spacing predicted from a 15° molecular tilt. This is quite close to the same direction ($\Phi = 27°$ *versus* $\Phi = 25°$) of the smallest NN spacing observed for the ODT SAM on GaAs(110). Furthermore, along the [100] direction, every two lattice spacings of the ODT SAM ($d = 8.55$ Å) coincide with ~1.5 × the unit cell dimension ($d = 8.40$ Å) in this direction. As a result, rows of ODT molecules can nearly align with the zigzag rows that run perpendicular to the [100] direction. Thus, the pseudohexagonal superlattice of the ODT SAMs seems to originate from the molecules trying to simultaneously accommodate specific binding sites along multiple directions with multiple NN neighbor distances. Due to this complexity, it is not surprising that the incommensurate SAMs have small correlation lengths (~60 Å).

The preference for adsorbates to align along the zigzag rows is not without precedence. Dodecanethiolate monolayers on InP(110) have been reported to align along the these rows, with their chains tilted toward the [001] direction.[77,79] Scanning probe studies of single-walled carbon nanotubes adsorbed on GaAs(110) and InAs(110) surfaces also have similar alignment.[97]

Finally, the GIXRD measurements show that the ODT domains on the (110) surface preferentially align along the [200] direction of the rectangular intrinsic unit cell, which coincides with the dominant step edge direction. As with the previous case of the (001) monolithic substrate surface in which the monolayer domains align along the dominant step edge [110] direction of the substrate,[52] it appears that the domain growth in the (110) case is preferentially nucleated at step edges.

Comparison of Chemisorption on the (111-A)-Ga *versus* (111-B)-As Surfaces. All of the data for the ODT SAM on GaAs(111-B), As-rich surface support a hexagonally ordered structure with conformationally ordered chains at a near vertical orientation, though the SAM lattice spacing does not conform to any commensurate superlattice for the instrinic (111-B) lattice. Since the XPS data and general SAM stability are consistent with the formation of S−As bonding, it appears that the strong molecular packing forces between the chemisorbed alkanethiolate chains, coupled to the substrate lattice *via* the chemisorptions bonds, drive the SAM structure to a final preferred hexagonal symmetry at the cost of imposing lateral distortion of the intrinsic substrate lattice spacing. The short SAM domain correlation length of ~70 Å is consistent with this adsorbate-induced substrate surface strain. The tendency for the hexagonal SAM domains to incorporate orientational alignment with the intrinsic hexagonal substrate unit cell, as shown by alignment with the $[1\bar{1}0]$ direction, appears to be due to growth from step edges on the substrate.

In contrast, while the GIXRD data also support formation of a incommensurate hexagonal symmetry SAM on the (111-A), Ga-rich surface, the alignment with the substrate intrinsic unit cell directions is lost and the diffraction spots are considerably weaker than for the (111-B) case. Further, the IRS, XPS, and NEXAFS results indicate that the chain conformational order and coverage are lower than typical well-organized SAMs, although the surfaces remain quite hydrophobic and oleophobic from contact angle measurements. These data combined suggest that only a few ordered domains may be scattered across the surface while the major component of the SAM consists of large, interspersed regions with lower coverages and considerable disorder. This would support the observation of diffi-

culty in fitting the IRS spectra with even a single all-*trans* chain model.

The differences between the SAM structures on the Ga- and As-terminated (111) surfaces indicate an inherent difference in the ability of molecular packing forces to strain the two lattices. In both cases, S substrate bonds are formed, providing strong coupling of the adsorbates to the substrate lattice. In fact, previous evidence shows that the Ga−S bond is actually stronger than the As−S bond for GaAs surface bonding.[98] The noticeably poorer organization for the (111-A)-Ga case compared to the (111-B)-As and other faces indicates intrinsic differences in the abilities of the Ga and the As surface lattices to respond to the applied stresses of the chain organization forces, most likely with the Ga surface layer more resistant to restructuring, consistent with the generally higher stability of Ga *versus* As termination for GaAs.[66,67] In the limit of a completely rigid intrinsic Ga surface lattice with 3.995 Å NN spacings, given the ~4.5 Å diameters of the extended ODT chains, the closest packed ODT superlattice would be a $(\sqrt{3} \times \sqrt{3})R30°$ structure with chain tilts of ~50° and 6.92 Å NN adsorbate distances. An approach to this structure would account for the larger chain tilt angles for the Ga case, but we note that the apparent heterogeneity of the SAM structure (see above) indicates that the lattice strain is not uniform across the surface, resulting in both the formation of both ordered and disordered SAM domains.

CONCLUSIONS

In this study, octadecanethiol has been used as a constant adsorbate molecule for self-assembly on different crystal faces of GaAs, ranging from (001) and (110) with intrinsic square and rectangular symmetries, respectively, to the Ga-terminated (111-A) and As-terminated (111-B) intrinsic hexagonal symmetry faces. The main finding is that the molecular lattices all exhibit a hexagonal type of symmetry, regardless of the underlying intrinsic substrate lattice symmetry, while the specific adsorbate spacings, even for the hexagonal cases, do not match the underlying intrinsic substrate lattice spaces. In agreement with our previous conclusion on the GaAs(001) SAM, these results definitively show that the molecular organization is driven primarily by the intermolecular forces between the C18 alkyl chains to force the assembly toward a close-packed hexagonal structure, such as would occur in the limit on a perfectly featureless surface, such as a liquid. The strong coupling of the molecular chains to the substrate atoms *via* chemical bonding propagates stress into the substrate surface lattice. In each substrate case, the interatomic forces between the Ga and As atoms are insufficient to serve as a rigid template for the SAM organization, and the substrate surface lattice undergoes strain with each type of substrate lattice reaching a limit of strain that approaches but does not achieve the ideal SAM hexagonal structure. The noticeably poorer organization for the (111-A)-Ga case compared to the (111-B)-As and other faces indicates there are differences in the ability of the two surfaces to respond to the stresses with the Ga-terminated surface apparently more resistant to strain, resulting in a heterogeneous adsorbate structure, perhaps dependent on defects. Experiments with *epi*-GaAs(001) substrates show that the SAM domains exhibit no preferential alignment to the intrinsic substrate lattice directions, thus supporting the conclusion that dominant steps on a given surface trigger SAM nucleation, presumably due to lower activation barriers for dissociative chemisorption at step edges. Overall, the results of this study demonstrate the strong driving forces that intermolecular packing interactions can exert in determining the final self-organized assembly structures for cases of soft substrates such as heterocompound semiconductors. In this sense, one should consider both the surface and adsorbates as forming a new quasi-2D chemical product, which has a unique structure that neither of the reactants could achieve as isolated species, reminiscent of the well-known strong surface lattice reconstruction effects that can occur upon chemisorption of reactive atoms on transition metal surfaces.[99] In the present case, it is the strong intermolecular interactions from the large number of molecule−molecule contact points along the chains that drive the reconstruction forces. Exploration of such effects in other types of heterocompound semiconductors over a wide range of materials of technological interest is underway in our laboratories.

EXPERIMENTAL METHODS

Materials. Octadecanethiol (ODT), $CH_3[CH_2]_{17}SH$, was obtained from Aldrich Chemical Co. (Milwaukee, WI) and used as received. Four types of GaAs substrates were used for monolayer formation: single side polished n^+-type doped (100), (110), (111-A)-Ga, and (111-B)-As wafers, (2 in., Si dopant, 0.8−4 × 10^{18}/cc, prime epi-ready grade, American Xtal Technologies, Fremont, CA). Full 2 in. wafers were used for infrared spectroscopy, single wavelength ellipsometry, contact angle, and grazing incidence measurements; for all other characterizations, the wafers were cleaved into ~1 × 1 cm^2 shards.

Epitaxial GaAs surfaces were grown *via* surface quantum well (QW) structures fabricated at high temperature (580 °C) using molecular beam epitaxy (MBE) on (001) semi-insulating, epi-ready GaAs substrates, under As overpressure. First, a 170 nm thick GaAs buffer was grown after the desorption of the oxide layer on the substrate. Next, a 100 nm $Al_xGa_{1-x}As$ ($x \sim 0.4$) was grown to form the energy barrier on one side of the QW. Finally, a 10 nm GaAs QW was deposited on top of $Al_xGa_{1-x}As$.

Ethanol (Pharmco, ACS/USP grade) was degassed through multiple freeze−pump−thaw cycles and stored in a closed container in a nitrogen gas purged glovebox between uses. Water was purified to remove organic and ion impurities (Milli-Q grade

water; Millipore Products, Bedford, MA). Ammonium hydroxide (JT Baker, CMOS grade, 30% NH_4OH in water) and hexadecane (Sigma-Aldrich, 99$^+$% anhydrous) were used as received.

Monolayer Assembly. All monolayers were assembled according to the standard method described previously.[62] Briefly, the native oxide of GaAs was removed by immersing the substrates in concentrated NH_4OH from 1−5 min. Immediately after immersion, the sample was rinsed with anhydrous ethanol, dried with a N_2 stream, immediately immersed in degassed ethanolic solutions containing 3 mM ODT and ~10 m M NH_4OH, and rapidly transferred within 1 min into a nitrogen purged glovebox (O_2 < 5 ppm) for incubation for at least 20 h. After incubation, the samples were removed from solution, dried with N_2, and removed from the glovebox for immediate characterization or packaged under Ar in the dark for later analysis. Extended storage for several weeks under these conditions did not affect the analysis results. Once complete analysis was finished for a given sample, the sample was recycled for use by exposure to UV−ozone to remove the monolayer and regrow an oxide layer. The oxide was subsequently removed by etching of NH_4OH. Use of recycled substrates gave identical results to those with fresh substrates. The surface morphologies and surface characteristics of the native oxide and NH_4OH etched substrates were identical to those previously reported.[38,52,62]

Contact Angle Measurements. Sessile drop measurements were made using a home-built apparatus with a CCD camera which captures drop images digitally. The contact angles were analyzed using ImageJ software (National Institutes of Health, USA). A 20 μL drop was dispensed on the surface with a flat tipped micrometer syringe (GS-1200, Gilmont Instruments, Barrington, IL) for each of the two probe liquids, Milli-Q water and hexadecane (HD). The drop was then pulled at a rate of 50 μm/s across the surface using a piezoelectric micromanipulator to determine the advancing and receding angles. This method has been reported to return an angle somewhere between the max advancing angle and the equilibrium contact angle.[100] A minimum of three measurements were made at different spots for each sample, and at least three samples were tested for each probe liquid.

Near-Edge X-ray Absorption Fine Structure (NEXAFS). The fabricated films were characterized by angle-resolved NEXAFS spectroscopy at the HE-SGM beamline of the synchrotron storage ring BESSY II in Berlin, Germany. The results were compared with the analogous data set for a hexadecanethiolate SAM on Au{111} (HDT/Au), which served as reference sample. During analysis, the samples remained at room temperature and a base pressure of 1.5×10^{-9} mbar. The spectra acquisition time was selected in such a way that no noticeable damage by the primary X-rays occurred during the measurements.[101−104]

Spectral acquisition was carried out at the C *K*-edge in the partial electron yield mode with a retarding voltage of −150 V. Linear polarized synchrotron light with a polarization factor of ~0.82 was used. The energy resolution was ~0.40 eV. The incidence angle of the X-ray light was varied from 90° (***E***-vector in surface plane) to 20° (***E***-vector near surface normal) in steps of 10−20° to monitor the orientational order in the SAMs.

The raw spectra of ODT/GaAs and HDT/Au were normalized to the incident photon flux by division with a spectrum of a clean, freshly sputtered gold sample. In the case of ODT/GaAs, a raw spectrum of freshly sputtered GaAs was subtracted from the raw spectrum of SAM-covered sample before the normalization, with both spectra being normalized to the pre-edge intensity.[105] Further, the spectra were reduced to the standard form by subtracting linear pre-edge background and normalizing to the unity edge jump determined by a horizontal plateau 40−50 eV above the absorption edge. The energy scale was referenced to the pronounced π* resonance of highly oriented pyrolytic graphite at 285.38 eV.[87]

X-ray Photoelectron Spectroscopy (XPS). High-resolution XPS (HRXPS) measurements were carried out at the D1011 beamline of the synchrotron storage ring MAX II at MAX-Lab in Lund, Sweden, at room temperature and a base pressure lower than 1.5×10^{-9} Torr. The spectra (Ga 3d, As 3d, C 1s, O 1s, and S 2p) were collected by a SCIENTA analyzer in normal emission geometry. Excitation energies in the range of 130−580 eV were used. The choice of photon energy (PE) for a particular spectrum was based on the optimization of the photoionization cross section for the corresponding core level[106−108] and on adjustment of either surface or bulk sensitivity. The spectra acquisition time was selected in such a way that no noticeable damage by the primary X-rays occurred during the measurements.[101−104]

The energy resolution was better than 100 meV, allowing a clear separation of individual spectral components. The energy width of the individual emissions was close to the intrinsic energy spread of the respective core level photoemission process. Energy calibration was performed individually for every spectrum to avoid effects related to the instability of the monochromator. The binding energy (BE) scale of every spectrum was individually calibrated using the Au $4f_{7/2}$ emission line of a dodecanethiolate (DDT)-covered Au substrate at 83.95 eV. The latter value is given by the latest ISO standard.[109] It is very close to a value of 83.93 eV, which has been obtained by us for Au $4f_{7/2}$ using a separate calibration to the Fermi edge of a clean Pt foil.[103,110]

The decomposition of the HRXPS spectra was performed self-consistently over the entire data set. The spectra were fitted using Voigt peak profiles and a Shirley background. To fit the doublet emissions (Ga 3d, As 3d, and S 2p), we used two peaks with the same full width at half-maximum (fwhm), a reasonable spin−orbit splitting verified by fit, and branching ratios of 2:1 ($2p_{3/2}/2p_{1/2}$) and 3:2 ($3d_{5/2}/3d_{3/2}$). Due to the ultimate energy resolution and the presence of the spectra dominated by a single doublet, we were able to derive the initial setting for the respective parameters directly from the spectra and apply these settings to every individual doublet. The resulting accuracy of the binding energies (BE) and full widths at half-maximum of the peaks reported here is 0.04−0.05 eV. These values are noticeably lower than the ultimate accuracy of the experimental setup (see, *e.g.*, ref 111); they mostly reflect the distribution of the resulting fit parameters over the spectra of different samples.

For the *epi*-GaAs samples, lower-resolution XPS analyses were performed on a monochromatic Al Kα source instrument (Kratos, Axis Ultra; England) operating with a pass energy of 20 eV and an energy step of 0.15 eV. These conditions resulted in a fwhm of 0.71 eV for the Au $4f_{7/2}$ line at 84.0 eV with an average instrumental resolution of ~0.8 eV. For internal referencing of C 1s positions, we chose the bulk As $3d_{5/2}$ peak. In all cases, collection times were shorter than the onset of noticeable film degradation determined by comparing survey spectra before and after data collection. Data were collected at a take off angle of 90° from the surface and analyzed using the CASA XPS Analysis program (Neil Farley, Casa XPS). All spectra were referenced to the As $3d_{5/2}$ peak at 40.95 eV.

Infrared Reflection Spectroscopy. The IR spectra were collected using a custom, in-house modified FTIR spectrometer (BioRad FTS-7000/Digilab, Randolph, MA) with sample−detector optics mounted on a goniometer and housed in an external N_2 or dry air (H_2O- and CO_2-free) purge box.[112] The θ−2θ goniometer allowed continuous selection of angles of incidence from ~87 to ~20° without reconfiguring the optical train. The signal was collected and focused into a liquid N_2-cooled mercury cadmium telluride (MCT) broad band detector. Spectra were obtained at 4 cm^{-1} resolution in order to avoid interference fringes that occur due to multiple back reflections (fringing) within the crystal faces of the GaAs wafers. Scans were collected at 20 kHz, and the interferograms were transformed using triangular apodization with zero filling for increased point density where needed. The incident beam was p-polarized and set at either 80 or 55° angles of incidence (AOI) from the surface normal. For large (>1.5 in.) samples, 80° AOI was used to accommodate a large beam spread. For samples too small to accommodate this beam spread (*e.g.*, *epi*-GaAs samples), a 55° AOI was used. It has previously been established that these two angles have approximately the same signal-to-noise ratio.[62] Typically ~2000 scans were co-added to improve the signal-to-noise. Spectral intensities are reported as $-\log(I/I_0)$, where I is the output power of the IR beam from the samples and I_0 is the output power from a reference sample. The most useful reference was a bare GaAs substrate used immediately after oxide removal to minimize contamination. Experimental details have been described previously.[62]

IRS Spectral Simulations. Simulations of the IRS spectra for the SAMs on GaAs were modeled using a rigorous, full scale implementation of the 4 × 4 transfer matrix method developed by Yeh[113] and extended by Parikh and Allara for organic thin film applications.[112] Since GaAs is a semiconducting substrate, the poor conductivity leads to very little screening of the surface components of the electric field, and as a result, both parallel and perpendicular components of vibrations of the molecules can be excited.[114] This necessitates determination of all matrix elements of the optical functions.

For reflection measurements using IR opaque, doped GaAs, the SAM structures were modeled as a two-layer planar stack with an optically infinite, isotropic substrate and a uniaxially anisotropic SAM (oriented chains with no preferential direction in the surface plane). The GaAs optical function spectra were obtained by interpolating values found from literature.[115] The SAM optical tensor spectra for each selected chain orientation (tilt) were constructed by scaling experimentally obtained isotropic *k* spectra of the molecule by the directional cosines of the transition dipole moments of each mode. Spectra were simulated for any chosen SAM thickness, chain tilt, and AOI using codes developed by Parikh and Allara.[112] The calculations yielded reflectivities of the bare substrate (R_0) and SAM-covered substrates (R). The final absorbance spectra were calculated as $-\log(R/R_0)$. A wide variety of model structures were used as inputs to the simulations, and the best fit to experimental spectra provided a basis for characterizing the structure of each SAM.

Grazing Incidence X-ray Diffraction (GIXRD). Diffraction patterns were obtained at the G-2 beamline at the Cornell High Energy Synchrotron Source (CHESS) using a 100 mm position sensitive linear gas detector (Ordela, Inc., Oak Ridge, TN) with a matching large Soller collimator (JJ X-ray, Denmark) which detects exit angle spectra at specific in-plane scattering angles.[116] Each sample was mounted onto a six-circle κ diffractometer[117] and enclosed in a He purged cylindrical Mylar cell, to protect the monolayers from oxidation and to minimize localized X-ray damage. An X-ray wavelength of 1.2047 Å was selected using a side-bounce beryllium single crystal, and the beam was collimated to 0.2 mm height and 5 mm width, by two sets of slits. The in-plane azimuth direction was calibrated by aligning along the GaAs [220] direction.[118] For the radial scans parallel to the surface, a resolution of $\Delta q_{xy} = \sim 0.02$ Å^{-1} was used. For azimuth scans, an angular resolution of $\Delta\phi = 1°$ was used. Each exit angle spectrum took ~60−200 s to collect, depending on the beam intensity. Under these conditions, we found that main monolayer structure is insensitive to X-ray exposure; that is, the integrated X-ray scattering intensity and diffraction positions did not vary within the typical 48 h that each sample was exposed to the X-ray beam. However, as the monolayer exposure time to the X-ray beam increased, we found evidence of new, sharp diffraction peaks growing in, presumably due to a new X-ray-induced monolayer structure. Post-analysis of the samples revealed degradation in the monolayer wetting properties and IRS intensities. All peak positions were determined by fitting the 2D integrated intensity to a Lorentzian line shape.[119] To enhance surface sensitivity, GIXRD measurements were performed at a grazing angle of $\alpha = 0.15°$ with respect to the surface plane. This angle is below the critical angle for total external reflection from the GaAs substrate (0.3°), so in this scattering geometry, the incident wavevector, **k**, is essentially in the plane of the surface. The exit wave vector, **k**′, and thus the scattering vector, **Q**, has components parallel to the surface and perpendicular to the surface; q_{xy} characterizes the packing of the alkyl chains, while the q_z dependence of the scattering provides information about the tilt of the chains.[9,52]

Acknowledgment. The authors gratefully acknowledge financial support from the NSF funded Pennsylvania State University Center for Nanoscale Science (MRSEC Grant DMR-0080019; C.L.M. and D.L.A.) and the German BMBF (05KS4VHA/4) and the European Community IA-SFS project (A.S., T.W., and M.Z.). Part of this work is based upon research conducted at the Cornell High Energy Synchrotron Source (CHESS), which is supported by the National Science Foundation and the National Institutes of Health/National Institute of General Medical Sciences under NSF Award DMR-0225180.

Supporting Information Available: As 3d and Ga 3d XPS core level spectra of oxide peaks, contact angle, and IRS and XPS measurements on ODT SAMs assembled on *epi*-GaAs(001) substrates. This material is available free of charge *via* the Internet at http://pubs.acs.org.

REFERENCES AND NOTES

1. Kacker, N.; Kumar, S. K.; Allara, D. L. Wetting-Induced Reconstruction in Molecular Surfaces. *Langmuir* **1997**, *13*, 6366–6369.
2. Parikh, A. N.; Liedberg, B.; Atre, S. V.; Ho, M.; Allara, D. L. Correlation of Molecular Organization and Substrate Wettability in the Self-Assembly of *n*-Alkylsiloxane Monolayers. *J. Phys. Chem.* **1995**, *99*, 9996–10008.
3. Allara, D. L.; Parikh, A. N.; Judge, E. The Existence of Structure Progressions and Wetting Transitions in Intermediately Disordered Monolayer Alkyl Chain Assemblies. *J. Chem. Phys.* **1994**, *100*, 1761–1764.
4. Abbott, N. L.; Gorman, C. B.; Whitesides, G. M. Active Control of Wetting Using Applied Electrical Potentials and Self-Assembled Monolayers. *Langmuir* **1995**, *11*, 16–18.
5. Haran, A.; Waldeck, D. H.; Naaman, R.; Moons, E.; Cahen, D. The Dependence of Electron Transfer Efficiency on the Conformational Order in Organic Monolayers. *Science* **1994**, *263*, 948–950.
6. Salomon, A.; Cahen, D.; Lindsay, S.; Tomfohr, J.; Engelkes, V. B.; Frisbie, C. D. Comparison of Electronic Transport Measurements on Organic Molecules. *Adv. Mater.* **2003**, *15*, 1881–1890.
7. Mrksich, M.; Whitesides, G. M. Using Self-Assembled Monolayers To Understand the Interactions of Man-Made Surfaces with Proteins and Cells. *Annu. Rev. Biophys. Biomol. Struct.* **1996**, *25*, 55–78.
8. Whaley, S. R.; English, D. S.; Hu, E. L.; Barbara, P. F.; Belcher, A. M. Selection of Peptides with Semiconductor Binding Specificity for Directed Nanocrystal Assembly. *Nature* **2000**, *405*, 665–668.
9. Kaganer, V. M.; Mohwald, H.; Dutta, P. Structure and Phase Transitions in Langmuir Monolayers. *Rev. Mod. Phys.* **1999**, *71*, 779–819.
10. Kaganer, V. M.; Peterson, I. R.; Kenn, R. M.; Shih, M. C.; Durbin, M.; Dutta, P. Tilted Phases of Fatty Acid Monolayers. *J. Chem. Phys.* **1995**, *102*, 9412–9422.
11. Dudowicz, J.; Douglas, J. F.; Freed, K. F. An Exactly Solvable Model of Hierarchical Self-Assembly. *J. Chem. Phys.* **2009**, *130*, 224906–224908.
12. Love, J. C.; Estroff, L. A.; Kriebel, J. K.; Nuzzo, R. G.; Whitesides, G. M. Self-Assembled Monolayers of Thiolates on Metals as a Form of Nanotechnology. *Chem. Rev.* **2005**, *105*, 1103–1169.
13. Ulman, A. Formation and Structure of Self-Assembled Monolayers. *Chem. Rev.* **1996**, *96*, 1533–1554.
14. Linford, M. R.; Chidsey, C. E. D. Alkyl Monolayers Covalently Bonded to Silicon Surfaces. *J. Am. Chem. Soc.* **1993**, *115*, 12631–12632.
15. Linford, M. R.; Fenter, P.; Eisenberger, P. M.; Chidsey, C. E. D. Alkyl Monolayers on Silicon Prepared from 1-Alkenes and Hydrogen-Terminated Silicon. *J. Am. Chem. Soc.* **1995**, *117*, 3145–3155.
16. Smilgies, D.-M.; Kintzel, J. E. J. Epitaxial Orientations of *para*-Sexiphenyl Platelets Grown on Alkali Halide (001) Surfaces. *Phys. Rev. B* **2009**, *79*, 235413-10.
17. Schollmeyer, H.; Struth, B.; Riegler, H. Long Chain *n*-Alkanes at SiO_2/Air Interfaces: Molecular Ordering, Annealing, and Surface Freezing of Triacontane in the Case of Excess and Submonolayer Coverage. *Langmuir* **2003**, *19*, 5042–5051.
18. Bigelow, W. C.; Pickett, D. L.; Zisman, W. A. Oleophobic Monolayers. I. Films Adsorbed from Solution in Non-polar Liquids. *J. Colloid. Sci.* **1946**, *101*, 201.
19. Maoz, R.; Sagiv, J. J. On the Formation and Structure of Self-Assembling Monolayers. I. A Comparative ATR-

Wettability Study of Langmuir−Blodgett and Adsorbed Films on Flat Substrates and Glass Microbeads. *Colloid Interface Sci.* **1984**, *100*, 465–496.
20. Parikh, A. N.; Allara, D. L.; Azouz, I. B.; Rondelez, F. An Intrinsic Relationship between Molecular Structure in Self-Assembled *n*-Alkylsiloxane Monolayers and Deposition Temperature. *J. Phys. Chem.* **1994**, *98*, 7577–7590.
21. Tidswell, I. M.; Rabedeau, T. A.; Pershan, P. S.; Kosowsky, S. D.; Folkers, J. P.; Whitesides, G. M. X-ray Grazing Incidence Diffraction from Alkylsiloxane Monolayers on Silicon Wafers. *J. Chem. Phys.* **1991**, *95*, 2854–2861.
22. Nuzzo, R. G.; Zegarski, B. R.; Dubois, L. H. Fundamental Studies of the Chemisorption of Organosulfur Compounds on Gold(111). Implications for Molecular Self-Assembly on Gold Surfaces. *J. Am. Chem. Soc.* **1987**, *109*, 733–740.
23. Nuzzo, R. G.; Dubois, L. H.; Allara, D. L. Fundamental Studies of Microscopic Wetting on Organic Surfaces. 1. Formation and Structural Characterization of a Self-Consistent Series of Polyfunctional Organic Monolayers. *J. Am. Chem. Soc.* **1990**, *112*, 558–569.
24. Schreiber, F. Structure and Growth of Self-Assembling Monolayers. *Prog. Surf. Sci.* **2000**, *65*, 151–256.
25. Camillone, N.; Chidsey, C. E. D.; Liu, G.-y.; Putvinski, T. M.; Scoles, G. Surface Structure and Thermal Motion of *n*-Alkane Thiols Self-Assembled on Au(111) Studied by Low Energy Helium Diffraction. *J. Chem. Phys.* **1991**, *94*, 8493–8502.
26. Camillone, N.; Eisenberger, P.; Leung, T. Y. B.; Schwartz, P.; Scoles, G.; Poirier, G. E.; Tarlov, M. J. New Monolayer Phases of *n*-Alkane Thiols Self-Assembled on Au(111): Preparation, Surface Characterization, and Imaging. *J. Chem. Phys.* **1994**, *101*, 11031–11036.
27. Poirier, G. E.; Pylant, E. D. The Self-Assembly Mechanism of Alkanethiols on Au(111). *Science* **1996**, *272*, 1145–1148.
28. Torrelles, X.; Barrena, E.; Munuera, C.; Rius, J.; Ferrer, S.; Ocal, C. New Insights in the $c(4 \times 2)$ Reconstruction of Hexadecanethiol on Au(111) Revealed by Grazing Incidence X-ray Diffraction. *Langmuir* **2004**, *20*, 9396–9402.
29. Fenter, P.; Eisenberger, P.; Liang, K. S. Chain-Length Dependence of the Structures and Phases of CH_3CH_2)-*n*-ish Self Assembled on Au(111). *Phys. Rev. Lett.* **1993**, *70*, 2447–2450.
30. Poirier, G. E. Mechanism of Formation of Au Vacancy Islands in Alkanethiol Monolayers on Au(111). *Langmuir* **1997**, *13*, 2019–2026.
31. Donhauser, Z. J.; Price, D. W., Il; Tour, J. M.; Weiss, P. S. Control of Alkanethiolate Monolayer Structure Using Vapor-Phase Annealing. *J. Am. Chem. Soc.* **2003**, *125*, 11462–11463.
32. Barrena, E.; Ocal, C.; Salmeron, M. *J. Chem. Phys.* **1999**, *111*, 9797–9802.
33. Poirier, G. E. Coverage-Dependent Phases and Phase Stability of Decanethiol on Au(111). *Langmuir* **1999**, *15*, 1167–1175.
34. Han, S. M.; Ashurst, W. R.; Carraro, C.; Maboudian, R. Formation of Alkanethiol Monolayer on Ge(111). *J. Am. Chem. Soc.* **2001**, *123*, 2422–2425.
35. He, J. L.; Lu, Z. H.; Mitchell, S. A.; Wayner, D. D. M. Self-Assembly of Alkyl Monolayers on Ge(111). *J. Am. Chem. Soc.* **1998**, *120*, 2660–2661.
36. Ardalan, P.; Musgrave, C. B.; Bent, S. F. Formation of Alkanethiolate Self-Assembled Monolayers at Halide-Terminated Ge Surfaces. *Langmuir* **2009**, *25*, 2013–2025.
37. Buriak, J. M. Organometallic Chemistry on Silicon and Germanium Surfaces. *Chem. Rev.* **2002**, *102*, 1271–1308.
38. McGuiness, C. L.; Shaporenko, A.; Zharnikov, M.; Walker, A. V.; Allara, D. L. Molecular Self-Assembly at Bare Semiconductor Surfaces: Investigation of the Chemical and Electronic Properties of the Alkanethiolate−GaAs(001) Interface. *J. Phys. Chem. C* **2007**, *111*, 4226–4234.
39. Sheen, C. W.; Shi, J. X.; Martensson, J.; Parikh, A. N.; Allara, D. L. A New Class of Organized Self-Assembled Monolayers: Alkane Thiols on Gallium Arsenide(100). *J. Am. Chem. Soc.* **1992**, *114*, 1514–1515.
40. Adlkofer, K.; Eck, W.; Grunze, M.; Tanaka, M. Surface Engineering of Gallium Arsenide with 4-Mercaptobiphenyl Monolayers. *J. Phys. Chem. B* **2003**, *107*, 587–591.
41. Adlkofer, K.; Shaporenko, A.; Zharnikov, M.; Grunze, M.; Ulman, A.; Tanaka, M. Chemical Engineering of Gallium Arsenide Surfaces with 4′-Methyl-4-mercaptobiphenyl and 4′-Hydroxy-4-mercaptobiphenyl Monolayers. *J. Phys. Chem. B* **2003**, *107*, 11737–11741.
42. Lunt, S. R.; Santangelo, P. G.; Lewis, N. S. Passivation of GaAs Surface Recombination with Organic Thiols. *J. Vac. Sci. Technol., B* **1991**, *9*, 2333–2336.
43. Dorsten, J. F.; Maslar, J. E.; Bohn, P. W. Near-Surface Electronic Structure in GaAs (100) Modified with Self-Assembled Monolayers of Octadecylthiol. *Appl. Phys. Lett.* **1995**, *66*, 1755–1757.
44. Ke, Y.; Milano, S.; Wang, X. W.; Tao, N.; Darici, Y. Structural Studies of Sulfur-Passivated GaAs (100) Surfaces with LEED and AFM. *Surf. Sci.* **1998**, *415*, 29–36.
45. Adlkofer, K.; Tanaka, M. Stable Surface Coating of Gallium Arsenide with Octadecylthiol Monolayers. *Langmuir* **2001**, *17*, 4267–4273.
46. Li, W. J.; Kavanagh, K. L.; Matzke, C. M.; Talin, A. A.; Leonard, F.; Faleev, S.; Hsu, J. W. P. Ballistic Electron Emission Microscopy Studies of Au/Molecule/*n*-GaAs Diodes. *J. Phys. Chem. B* **2005**, *109*, 6252–6256.
47. Loo, Y. L.; Lang, D. V.; Rogers, J. A.; Hsu, J. W. P. Electrical Contacts to Molecular Layers by Nanotransfer Printing. *Nano Lett.* **2003**, *3*, 913–917.
48. Baum, T.; Ye, S.; Uosaki, K. Formation of Self-Assembled Monolayers of Alkanethiols on GaAs Surface with *In Situ* Surface Activation by Ammonium Hydroxide. *Langmuir* **1999**, *15*, 8577–8579.
49. Jun, Y.; Zhu, X. Y.; Hsu, J. W. P. Formation of Alkanethiol and Alkanedithiol Monolayers on GaAs(001). *Langmuir* **2006**, *22*, 3627–3632.
50. Rosu, D. M.; Jones, J. C.; Hsu, J. W. P.; Kavanagh, K. L.; Tsankov, D.; Schade, U.; Esser, N.; Hinrichs, K. Molecular Orientation in Octanedithiol and Hexadecanethiol Monolayers on GaAs and Au Measured by Infrared Spectroscopic Ellipsometry. *Langmuir* **2009**, *25*, 919–923.
51. (a) Stine, R.; Petrovykh, D. Y. Oriented Self-Assembled Monolayers of Bifunctional Molecules on InAs. *J. Electron Spectrosc. Relat. Phenom.* **2009**, *172*, 42–46. (b) Petrovykh, D. Y.; Smith, J. C.; Clark, T. D.; Stine, R.; Baker, L. A.; Whitman, L. J. Self-Assembled Monolayers of Alkanethiols on InAs. *Langmuir* **2009**, *25*, 12185.
52. McGuiness, C. L.; Blasini, D.; Masejewski, J. P.; Uppili, S.; Cabarcos, O. M.; Smilgies, D.; Allara, D. L. Molecular Self-Assembly at Bare Semiconductor Surfaces: Characterization of a Homologous Series of *n*-Alkanethiolate Monolayers on GaAs(001). *ACS Nano* **2007**, *1*, 30–49.
53. Dubois, L. H.; Zegarski, B. R.; Nuzzo, R. G. Molecular Ordering of Organosulfur Compounds on Au(111) and Au(100): Adsorption from Solution and in Ultrahigh Vacuum. *J. Chem. Phys.* **1993**, *98*, 678–688.
54. Chidsey, C. E. D.; Liu, G. Y.; Rowntree, P.; Scoles, G. Molecular Order at the Surface of an Organic Monolayer Studied by Low Energy Helium Diffraction. *J. Chem. Phys.* **1989**, *91*, 4421–4423.
55. Alves, C. A.; Smith, E. L.; Porter, M. D. Atomic Scale Imaging of Alkanethiolate Monolayers at Gold Surfaces with Atomic Force Microscopy. *J. Am. Chem. Soc.* **1992**, *114*, 1222–1227.
56. Poirier, G. E. Characterization of Organosulfur Molecular Monolayers on Au(111) Using Scanning Tunneling Microscopy. *Chem. Rev.* **1997**, *97*, 1117–1127.
57. Camillone, N.; Chidsey, C. E. D.; Liu, G. Y.; Scoles, G. Superlattice Structure at the Surface of a Monolayer of Octadecanethiol Self-Assembled on Au(111). *J. Chem. Phys.* **1993**, *98*, 3503–3511.
58. Ohtake, A.; Nakamura, J.; Komura, T.; Hanada, T.; Yao, T.; Kuramochi, H.; Ozeki, M. Surface Structures of GaAs{111}A,B-(2×2). *Phys. Rev. B* **2001**, *64*, 045318.
59. Laibinis, P. E.; Whitesides, G. M.; Allara, D. L.; Tao, Y. T.;

Parikh, A. N.; Nuzzo, R. G. Comparison of the Structures and Wetting Properties of Self-Assembled Monolayers of *n*-Alkanethiols on the Coinage Metal Surfaces, Copper, Silver, and Gold. *J. Am. Chem. Soc.* **1991**, *113*, 7152–7167.
60. Love, J. C.; Wolfe, D. B.; Haasch, R.; Chabinyc, M. L.; Paul, K. E.; Whitesides, G. M.; Nuzzo, R. G. Formation and Structure of Self-Assembled Monolayers of Alkanethiolates on Palladium. *J. Am. Chem. Soc.* **2003**, *125*, 2597–2609.
61. Li, Z. Y.; Chang, S. C.; Williams, R. S. Self-Assembly of Alkanethiol Molecules onto Platinum and Platinum Oxide Surfaces. *Langmuir* **2003**, *19*, 6744–6749.
62. McGuiness, C. L.; Shaporenko, A.; Mars, C. K.; Uppili, S.; Zharnikov, M.; Allara, D. L. Molecular Self-Assembly at Bare Semiconductor Surfaces: Preparation and Characterization of Highly Organized Octadecanethiolate Monolayers on GaAs(001). *J. Am. Chem. Soc.* **2006**, *128*, 5231–5243.
63. Camillone, N.; Chidsey, C. E. D.; Liu, G.; Scoles, G. Substrate Dependence of the Surface Structure and Chain Packing of Docosyl Mercaptan Self-Assembled on the (111), (110), and (100) Faces of Single Crystal Gold. *J. Chem. Phys.* **1993**, *98*, 4234–4245.
64. Ranke, W.; Jacobi, K. Structure and Reactivity of GaAs Surfaces. *Prog. Surf. Sci.* **1981**, *10*, 1–52.
65. Xue, Q. K.; Hashizume, T.; Sakurai, T. Scanning Tunneling Microscopy of III−V Compound Semiconductor (001) Surfaces. *Prog. Surf. Sci.* **1997**, *56*, 1–131.
66. Blakemore, J. S. Semiconducting and Other Major Properties of Gallium Arsenide. *J. Appl. Phys.* **1982**, *53*, R123–R181.
67. William, R. E. *Gallium Arsenide Processing Techniques*; Artech House, Inc.: Dedham, MA, 1984.
68. Ding, X. M.; Moumanis, K.; Dubowski, J. J.; Tay, L.; Rowell, N. L. Fourier-Transform Infrared and Photoluminescence Spectroscopies of Self-Assembled Monolayers of Long-Chain Thiols on (001) GaAs. *J. Appl. Phys.* **2006**, *99*, 54701.
69. Voznyy, O.; Dubowski, J. J. Structure, Bonding Nature, and Binding Energy of Alkanethiolate on As-Rich GaAs(001) Surface: A Density Functional Theory Study. *J. Phys. Chem. B* **2006**, *110*, 23619–23622.
70. Wieliczka, D. M.; Ding, X.; Dubowski, J. J. X-ray Photoelectron Spectroscopy of Self-Assembled Monolayers of Alkanethiols on (001) GaAs. *J. Vac. Sci. Technol., A* **2006**, *24*, 1756–1759.
71. Voznyy, O.; Dubowski, J. J. Structure of Thiol Self-Assembled Monolayers Commensurate with the GaAs (001) Surface. *Langmuir* **2008**, *24*, 13299–13305.
72. Voznyy, O.; Dubowski, J. J. Adsorption Kinetics of Hydrogen Sulfide and Thiols on GaAs (001) Surfaces in a Vacuum. *J. Phys. Chem. C* **2008**, *112*, 3726–3733.
73. Camillone, N.; Khan, K. A.; Osgood, R. M. The Thermal Chemistry of Model Organosulfur Compounds on Gallium Arsenide (110). *Surf. Sci.* **2000**, *453*, 83–102.
74. Ohno, H.; Motomatsu, M.; Mizutani, W.; Tokumoto, H. AFM Observation of Self-Assembled Monolayer Films on GaAs (110). *Jpn. J. Appl. Phys., Part 1* **1995**, *34*, 1381–1386.
75. Moumanis, K.; Ding, X.; Dubowski, J. J.; Frost, E. H. Aging and Detergent Washing Effects of the Surface of (001) and (110) GaAs Passivated with Hexadecanethiol. *J. Appl. Phys.* **2006**, *100*, 034702-5.
76. Rodriguez, L. M.; Gayone, J. E.; Sanchez, E. A.; Grizzi, O.; Blum, B.; Salvarezza, R. C.; Xi, L.; Lau, W. M. Gas Phase Formation of Dense Alkanethiol Layers on GaAs(110). *J. Am. Chem. Soc.* **2007**, *129*, 7807–7813.
77. Zerulla, D.; Chasse, T. Scanning Tunneling Microscopy and Spectroscopy of UHV-Deposited Dodecanethiolate Films on InP(110) Surfaces at Consecutive Doses: A Single Domain System. *Langmuir* **2002**, *18*, 5392–5399.
78. Zerulla, D.; Chasse, T. X-ray Induced Damage of Self-Assembled Alkanethiols on Gold and Indium Phosphide. *Langmuir* **1999**, *15*, 5285–5294.
79. Zerulla, D.; Mayer, D.; Hallmeier, K. H.; Chasse, T. T. Angular-Resolved XANES Measurements of the Polar and Azimuthal Orientation of Alkanethiols on InP(110). *Chem. Phys. Lett.* **1999**, *311*, 8–12.
80. Lindau, I.; Spicer, W. E. The Probing Depth in Photoemission and Auger-Electron Spectroscopy. *J. Electron Spectrosc. Relat. Phenom.* **1974**, *3*, 409–413.
81. Powell, C. J. Attenuation Lengths of Low-Energy Electrons in Solids. *Surf. Sci.* **1974**, *44*, 29–46.
82. Shaporenko, A.; Adlkofer, K.; Johansson, L. S. O.; Ulman, A.; Grunze, M.; Tanaka, M.; Zharnikov, M. Spectroscopic Characterization of 4′-Substituted Aromatic Self-Assembled Monolayers on GaAs (100) Surfaces. *J. Phys. Chem. B* **2004**, *108*, 17964–17972.
83. These measurements were performed on a monochromatic Al Kα source instrument (Kratos, Axis Ultra; England) operating with a pass energy of 20 eV.
84. Stohr, J. *NEXAFS Spectroscopy*; Springer-Verlag: Berlin, 1992.
85. Vaterlein, P.; Fink, R.; Umbach, E.; Wurth, W. Analysis of the X-ray Absorption Spectra of Linear Saturated Hydrocarbons Using the Xα Scattered-Wave Method. *J. Chem. Phys.* **1998**, *108*, 3313–3320.
86. Scholl, A.; Fink, R.; Umbach, E.; Mitchell, G. E.; Urquhart, S. G.; Ade, H. Towards a Detailed Understanding of the NEXAFS Spectra of Bulk Polyethylene Copolymers and Related Alkanes. *Chem. Phys. Lett.* **2003**, *370*, 834–841.
87. Batson, P. E. Carbon 1*s* Near-Edge-Absorption Fine Structure in Graphite. *Phys. Rev. B* **1993**, *48*, 2608–2610.
88. Bagus, P. S.; Weiss, K.; Schertel, A.; Woll, C.; Braun, W.; Hellwig, C.; Jung, C. Identification of Transitions into Rydberg States in the X-ray Absorption Spectra of Condensed Long-Chain Alkanes. *Chem. Phys. Lett.* **1996**, *248*, 129–135.
89. Weiss, K.; Bagus, P. S.; Woll, C. Rydberg Transitions in X-ray Absorption Spectroscopy of Alkanes: The Importance of Matrix Effects. *J. Chem. Phys.* **1999**, *111*, 6834–6845.
90. Outka, D. A.; Stohr, J.; Rabe, J. P.; Swalen, J. D. The Orientation of Langmuir−Blodgett Monolayers Using NEXAFS. *J. Chem. Phys.* **1988**, *88*, 4076–4087.
91. Hahner, G.; Kinzler, M.; Woll, C.; Grunze, M.; Scheller, M. K.; Cederbaum, L. S. Near Edge X-ray-Absorption Fine-Structure Determination of Alkyl-Chain Orientation: Breakdown of the "Building-Block" Scheme. *Phys. Rev. Lett.* **1991**, *67*, 851–854.
92. Hahner, G.; Kinzler, M.; Thummler, C.; Woll, C.; Grunze, M. Structure of Self-Organizing Organic Films: A Near Edge X-ray Absorption Fine Structure Investigation of Thiol Layers Adsorbed on Gold. *J. Vac. Sci. Technol., A* **1992**, *10*, 2758–2763.
93. Snyder, R. G.; Hsu, S. L.; Krim, S. Vibrational Spectra in the C−H Stretching Region and the Structure of the Polymethylene Chain. *Spectrochim. Acta* **1978**, *34A*, 395–406.
94. Nuzzo, R. G.; Korenic, E. M.; Dubois, L. H. Studies of the Temperature-Dependent Phase Behavior of Long Chain *n*-Alkyl Thiol Monolayers on Gold. *J. Chem. Phys.* **1990**, *93*, 767–773.
95. Additional in plane, sharp ($\Delta q_{xy} \sim 0.01$ Å^{-1}) Bragg peaks at $q_{xy} = 1.39$, 1.41, and 1.68 Å^{-1} were also observed growing in on the radial maps after significant (~12−24 h) X-ray beam exposure. These new, sharp diffraction peaks are presumably due to a new X-ray-induced monolayer structure, the emergence of which did not affect the broader, initial peaks associated with the main monolayer structure. Similar results have also previously been observed in the GIXRD characterization of ODT, dodecanethiol (DDT), and 4′-methylbiphenyl-4-thiol samples (MBT) (ref 52). The new, sharp Bragg reflections are present for all ODT SAMs analyzed, regardless of the GaAs surface examined, and seem to be more prevalent on samples where the thiolate monolayers self assemble well (*i.e.*, on the DDT, MBT, and ODT on GaAs(111-A)-Ga samples). Azimuthal scans of these sharp diffraction peaks are observed to have ring-like structures typically associated with powder diffraction patterns from unoriented crystallites. At present, the full effect of these peaks is not known, but work is underway to understand their growth and origin. Given the large difference in Δq_{xy}

compared to the main monolayer reflections, these peaks do not appear to be related to the main, pristine monolayer structure.
96. The Scherrer equation, $L = 0.89\lambda/B \cos \theta_B$, where λ is the X-ray wavelength, θ_B is the Bragg angle of the monolayer, and B is the fwhm of the scattering angle $2\theta_B$, was used to determine the domain size.
97. Ruppalt, L. B.; Albrecht, P. M.; Lyding, J. W. Atomic Resolution Scanning Tunneling Microscope Study of Single-Walled Carbon Nanotubes on GaAs(110). *J. Vac. Sci. Technol., B* **2004**, *22*, 2005–2007.
98. (a) Scimeca, T.; Muramatsu, Y.; Oshima, M.; Oigawa, H.; Nannichi, Y. *Phys. Rev. B* **1991**, *44*, 12927–12932. (b) Ohno, T.; Shiraishi, K. *Phys. Rev. B* **1990**, *42*, 11194–11197. (c) Lebedev, M. V.; Mayer, T.; Jaegermann, W. *Surf. Sci.* **2003**, *547*, 171–183. (d) Medvedev, Y. V. *Appl. Phys. Lett.* **1994**, *64*, 3458–3460. (e) Spindt, C. J.; Liu, D.; Miyano, K.; Meissner, P. L.; Chiang, T. T.; Kendelewicz, T.; Lindau, I.; Spicer, W. E. *Appl. Phys. Lett.* **1989**, *55*, 861–863.
99. For example, see: Somorjai, G. A. *J. Phys. Chem. B* **2002**, *106*, 9201–9213.
100. Bain, C. D.; Troughton, E. B.; Tao, Y. T.; Evall, J.; Whitesides, G. M.; Nuzzo, R. G. Formation of Monolayer Films by the Spontaneous Assembly of Organic Thiols from Solution onto Gold. *J. Am. Chem. Soc.* **1989**, *111*, 321–335.
101. Wirde, M.; Gelius, U.; Dunbar, T.; Allara, D. L. Modification of Self-Assembled Monolayers of Alkanethiols on Gold by Ionizing Radiation. *Nucl. Instrum. Methods Phys. Res., Sect. B* **1997**, *131*, 245–251.
102. Jager, B.; Schurmann, H.; Muller, H. U.; Himmel, H. J.; Neumann, M.; Grunze, M.; Woll, C. X-ray and Low Energy Electron Induced Damage in Alkanethiolate Monolayers on Au-Substrates. *Z. Phys. Chem.* **1997**, *202*, 263–272.
103. Heister, K.; Zharnikov, M.; Grunze, M.; Johansson, L. S. O.; Ulman, A. Characterization of X-ray Induced Damage in Alkanethiolate Monolayers by High-Resolution Photoelectron Spectroscopy. *Langmuir* **2001**, *17*, 8–11.
104. Zharnikov, M.; Grunze, M. Modification of Thiol-Derived Self-Assembling Monolayers by Electron and X-ray Irradiation: Scientific and Lithographic Aspects. *J. Vac. Sci. Technol., B* **2002**, *20*, 1793–1807.
105. Shaporenko, A.; Adlkofer, K.; Johansson, L. S. O.; Tanaka, M.; Zharnikov, M. Functionalization of GaAs Surfaces with Aromatic Self-Assembled Monolayers: A Synchrotron-Based Spectroscopic Study. *Langmuir* **2003**, *19*, 4992–4998.
106. Band, I. M.; Kharitonov, Y. I.; Trzhaskovskaya, M. B. Photoionization Cross Sections and Photoelectron Angular Distributions for X-ray Line Energies in the Range 0.132−4.509 keV Targets. *At. Data Nucl. Data Tables* **1979**, *23*, 443–505.
107. Goldberg, S. M.; Fadley, C. S.; Kono, S. Photoionization Cross-Sections for Atomic Orbitals with Random and Fixed Spatial Orientation. *J. Electron Spectrosc. Relat. Phenom.* **1981**, *21*, 285–363.
108. Yeh, J. J.; Lindau, I. Atomic Subshell Photoionization Cross Sections and Asymmetry Parameters. *At. Data Nucl. Data Tables* **1985**, *32*, 1–155.
109. *Surface Chemical Analysis - X-ray Photoelectron Spectrometers - Calibration of the Energy Scales*; ISO 15472: 2001, **2006**.
110. Heister, K.; Zharnikov, M.; Grunze, M.; Johansson, L. S. O. Adsorption of Alkanethiols and Biphenylthiols on Au and Ag Substrates: A High-Resolution X-ray Photoelectron Spectroscopy Study. *J. Phys. Chem. B* **2001**, *105*, 4058–4061.
111. Heister, K.; Rong, H. T.; Buck, M.; Zharnikov, M.; Grunze, M.; Johansson, L. S. O. Odd−Even Effects at the S-Metal Interface and in the Aromatic Matrix of Biphenyl-Substituted Alkanethiol Self-Assembled Monolayers. *J. Phys. Chem. B* **2001**, *105*, 6888–6894.
112. Parikh, A. N.; Allara, D. L. Quantitative Determination of Molecular Structure in Multilayered Thin Films of Biaxial and Lower Symmetry from Photon Spectroscopies. I. Reflection Infrared Vibrational Spectroscopy. *J. Chem. Phys.* **1992**, *96*, 927–945.
113. Yeh, P. *Optical Waves in Layered Media*; Wiley-Interscience: New York, 1988.
114. Hecht, E. *Optics*; Addison Wesley: Reading, MA, 2001.
115. Palik, E. D. *Handbook of Optical Constants*; Academic Press: New York, 1985.
116. Smilgies, D. M.; Blasini, D. R.; Hotta, S.; Yanagi, H. Reciprocal Space Mapping and Single-Crystal Scattering Rods. *J. Synchrotron Radiat.* **2005**, *12*, 807–811.
117. Nowak, D. E.; Blasini, D. R.; Vodnick, A. M.; Blank, B.; Tate, M. W.; Deyhim, A.; Smilgies, D. M.; Abruna, H.; Gruner, S. M.; Baker, S. P. Six-Circle Diffractometer with Atmosphere- and Temperature-Controlled Sample Stage and Area and Line Detectors for Use in the G2 Experimental Station at CHESS. *Rev. Sci. Instrum.* **2006**, *77*, 113301.
118. The structure factor for reflections along a direction [*hkl*] when *hkl* are both odd and even numbers is zero for zinc blende crystals. The fcc structure factor is non-zero when *hkl* are all odd or all even with 0 considered even. In particular, (100) or (110) reflections are not observed. For example, see: Als-Nielson, J.; McMorrow, D. *Elements of Modern X-Ray Physics*; John Wiley & Sons: New York, 2001. For cubic crystals, high-symmetry directions are perpendicular to the corresponding Bragg planes. Hence measurements at the (200) and (220) substrate reflections identify the [100] and [110] directions, respectively.
119. Barton, S. W.; Thomas, B. N.; Flom, E. B.; Rice, S. A.; Lin, B.; Peng, J. B.; Ketterson, J. B.; Dutta, P. X-ray Diffraction Study of a Langmuir Monolayer of $C_{21}H_{43}OH$. *J. Chem. Phys.* **1988**, *89*, 2257–2270.